Pearlite Growth Rate in Fe-C Binary and Fe-X-C Ternary Steels

Seung-Woo Seo

Graduate Institute of Ferrous Technology, Pohang University of Science and Technology, Pohang 790-784, Republic of Korea

August 25, 2014

Contents

Nomenclature

α	Ferrite
$\bar{c}$	Average carbon content of the alloy
$\bar{D}$	Effective diffusivity of carbon in austenite lattice
$\Delta\epsilon$	Energy due to repulsive interaction between carbon atoms
ΔG	Gibbs free energy
ΔG_a	Activation free energy
ΔH	Latent heat of transformation
ΔH_{form}	Enthalpy change due to formation of vacancy
ΔH_{m}	Enthalpy change due to migration of vacancy
ΔS_{form}	Entropy change due to formation of vacancy
ΔS_{m}	Entropy change due to migration of vacancy
ΔT	Undercooling from the eutectoid temperature
δ	Depth of phase boundary
γ	Austenite

γ_m	Activity coefficient of the activated complex
λ	Distance between the austenite {002} planes
∇c_{C}	Carbon composition gradient at the pearlite/austenite interface
∇c_{C}	Gradient of X composition at the pearlite/austenite interface
ν	Attempt frequency
ρ	Density of pearlite
σ	Interfacial energy per unit area
$\sigma^{\alpha\theta}$	Interfacial energy per unit area of ferrite and cementite interface
θ	Cementite
a	Lattice constant
A^{α}	Cross sectional area of ferrite and austenite interface in pearlite
b	Arbitrary length of pearlite perpendicular to growth direction
$c^{\alpha\gamma}$	Concentration of solute at ferrite in equilibrium with austenite
$c^{\gamma\alpha}$	Concentration of solute at austenite in equilibrium with ferrite
$c^{\gamma\theta}$	Concentration of solute at austenite in equilibrium with cementite

$c^{\theta\gamma}$	Concentration of solute at cementite in equilibrium with austenite
c_γ	Mole fraction of carbon
$c_\gamma^{\gamma\alpha}$	Maximum permissible carbon content in the austenite at the transformation interface
D	Diffusion coefficient or Diffusivity
D_{C}^{γ}	Volume diffusion coefficient of carbon in austenite
D_{X}^{γ}	Volume diffusion coefficient of element X in austenite
D_{eff}^{i}	Effective diffusion coefficient of element i for mixed diffusion-controlled growth
D_0	Pre-exponential factor of diffusivity
D_B	Diffusion coefficient through phase boundary
D_V	Diffusion coefficient through the lattice
D_{C}^{γ}	Diffusion coefficient of carbon in austenite lattice
D_B^{C}	Boundary diffusion coefficient of carbon
D_B^{X}	Boundary diffusion coefficient of element X
D_V^{C}	Volume diffusion coefficient of carbon

D_V^{X}	Volume diffusion coefficient of element X
g	Geometric factor
h	Planck constant
J	Flux of solute during transformation
k	Boltzmann constant
Q	Activation energy for diffusion
Q_B	Activation energy for boundary diffusion
Q_V	Activation energy for volume diffusion
R_i	Weighted average of interface compositions for element i
S	Interlamellar spacing of pearlite
S^α	Length of the ferrite lamellae
S^θ	Length of the cementite lamellae
S_C	Critical interlamellar spacing of pearlite
T	Transformation temperature
T_e	Eutectoid temperature

v	Growth rate of pearlite
V_m	Molar volume of austenite
x_{C}	Mole fraction of carbon
Y_{C}	Site fraction of carbon
z	Coordination number of octahedral interstitial site in austenite
GB	Grain boundary
NPLE	Negligible partitioning local equilibrium
PLE	Partitioning local equilibrium

DFT Seung-Woo Seo

20110985 Pearlite growth rate in Fe-C Binary and

Fe-X-C Ternary Steels

Graduate Institute of Ferrous Technology (GIFT)

(Computational Metallurgy) 2015

Advisor: Prof. Dong Woo Suh;

Prof. H. K. D. H. Bhadeshia

Text in English

Abstract

The diffusion path during the pearlite transformation has been studied from the point of view of mixed diffusion-controlled growth. It is reasonable that the solutes do not choose only one path to move along when they have multiple available paths. This research has provided better fit for reported growth rate measurements of pearlite than volume and boundary diffusion models in isolation.

Local equilibrium is assumed to be maintained at ferrite/austenite and cementite/austenite interfaces. For the Fe-C binary system, the tie-lines which describe the interfacial compositions that maintain equilibrium at the interfaces are unique at a given temperature. Unlike the binary system, the local equilibrium condition in ternary system that contains an interstitial and substitutional solute needs to take account of the kinetic effect of solute because the complexity of the system is increased. Pearlite

transformation involves the cooperative growth of ferrite and cementite, thus, this also needs to be considered to find the appropriate local equilibrium condition. Two principles are required: one is mass conservation and the other is solute symmetry: the growth rate should have the same result when it is calculated by diffusion of any solute. The analysis is supported with transmission electron microscopy results and gives good agreement with Mn, Ni, and Co.

The local equilibrium condition for the pearlite transformation has been analysed for various diffusivity ratios of the two solutes and two different compositions. Two criteria can be distinguished when diffusivity ratio goes to infinity by observing the partitioning of substitutional solute between ferrite and cementite. The boundary between PLE and NPLE for pearlite is expected from the solution of the mixed diffusion equation.

1 Introduction

Pearlite contributes to the success of many commercial steels, for example those for rails, ropes for bridges and elevators, and tyre cords. In three dimensions, a colony of pearlite is an interpenetrating bi-crystal of cementite and ferrite [1], often approximated to consist of alternating lamellae of ferrite and cementite. The characteristic feature of pearlite is the fact that the ferrite (α) and cementite (θ) grow cooperatively, sharing a common transformation front with austenite (γ), where the excess carbon partitioned into the austenite as the ferrite grows, is absorbed by the adjacent cementite. The passage of this carbon occurs via the austenite at the transformation front, so the growth of the colony is modelled assuming that the rate is controlled by diffusion in the austenite ahead of the front [2, 3, 4, 5, 6]. Diffusion in the interface can be faster, and there are models for pearlite growth involving boundary diffusion control [7, 8]. There is of course, no reason why the solute is limited to either the volume or boundary, and there are models that deal simultaneously with both diffusion fluxes [9, 10, 11]. It has been suggested that diffusion behind the α/γ interface, towards the cementite, may also play a role [12], but this would lead to the thickening of the cementite behind the transformation front, and the evidence for such an effect is lacking. Strain resulting from the volume change has been claimed to cause a stress of 1000 MPa in the elastic limit, and only relieved by the diffusion of carbon. This stress driven diffusion thus accelerates the pearlite reaction [13]. The model is unphysical because it neglects the diffusion of iron that is necessary in a reconstructive transformation [14]; this relieves transformation strains including the volume change. In [13], the transformation in pure iron would be dramatically suppressed because to the absence of carbon diffusion, and this is patently not the case.

Assuming therefore, that the general problem is best treated by accounting for both the boundary and volume diffusion fluxes, there remain difficulties in dealing with ternary or higher order steels, especially if local equilibrium is assumed at the interphase boundaries. The well-known complication is that the diffusivities of the substitutional and interstitial solutes are vastly different, so unlike the case for binary steels, it becomes necessary to discover conditions where the two or more solute fluxes can keep pace whilst maintaining equilibrium locally at the interface [15, 16, 17, 18, 14]. This difficulty is discussed in more detail later in the text, but from an experimental point of view, there is no doubt that substitutional solutes are partitioned between the phases at all temperatures where pearlite is observed [19, 20, 21]. Pandit and Bhadeshia [11] found it necessary to make approximations when dealing with ternary alloys. Those estimations do not strictly satisfy the simultaneous conditions of local equilibrium and flux balance at all the interfaces involved in the growth of pearlite. In this thesis, an attempts is made to resolve this difficulty, bearing in mind that the kinetic theory for pearlite is of interest in many current scenarios [22, 23, 24, 25, 26, 27].

2 Literature Review

2.1 Austenite-Pearlite Reaction

Pearlite was discovered by Sorby [28] more than a century ago. Sorby described pearlite as a "the pearly compound" and assumed it has lamellar structure from the micrograph on the etched surface of pearlite. After the first observation, pearlite has been used for wide variety of purposes because it provides substantial contribution to strength, for example, tyre cord, rail, steel wires for bridge, and so on. Therefore pearlite has been studied intensively. Lamellar structure with two phases is not only observed in steel system but also it frequently reported in other metallic systems. So, pearlite is usually used for generic term to describe them.

2.2 The Morphology of Pearlite

100 years ago, Benedicks [29] noted that pro-eutectoid ferrite could act as a nucleus for pearlite as well as pro-eutectoid cementite. Smith and Mehl [30] found that ferrite in bainite had the same orientation relationship to parent austenite same as did Widmanstätten ferrite. Pearlitic ferrite does not show such kind of relationship. Hull and Mehl [31] conclude that pearlite starts to form from platelet of cementite and show a case where pearlitic cementite is always connected to proeutectoid cementite but pearlitic ferrite that grows from proeutectoid ferrite was never observed. This idea was challenged after Modin [32] reported that many micrographs had been published showing no proeutectoid ferrite/pearlitic ferrite boundaries. This was tested by Hillert and his colleagues by applying various metallographic techniques. They showed that pearlitic ferrite can have the same orientation with adjacent proeutectoid ferrite in a hypoeutectoid steels. In a

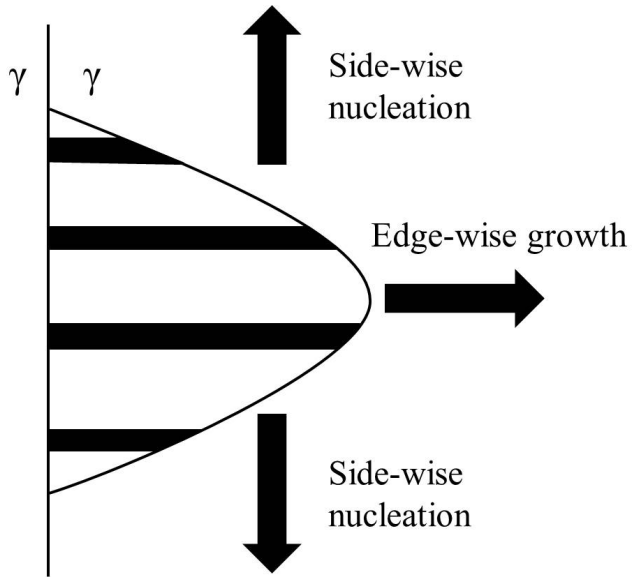

Figure 1: Edge-wise growth and side-wise nucleation nature of pearlite transformation. [32]

hypereutectoid system, pearlitic cementite can have same orientation as adjacent proeutectoid cementite.

The rapid increase in the number of lamellae after nucleation could be explained by edgewise growth into austenite grain and sidewise nucleation along the austenite grain boundary but also, Modin pointed out that it could be increased by branching inside of pearlite colony during growth. When pearlite nucleates on a grain boundary in between austenite, the direction that it grows is decided by interfacial energy. Pearlite nuclei form having orientation relationship with one of austenite grain. Obviously, the

other austenite will have an incoherent high-energy interface which has larger mobility than the other side of the nucleus. Therefore, pearlite grows toward the austenite grain with the high-energy interface. This was first pointed out by Smith. Hillert and his colleagues were able to show that pearlite did grow in this way, and on the other hand, Widmanstätten ferrite or cementite was usually observed to grow toward the low energy interface with austenite. It was proved by electron microscopy that pearlite/austenite interface is incoherent one. The interlamellar spacing in pearlite is the key factor of the strength of the pearlitic steels. It has been reported that extremely fine interlamellar spacing improves the pearlite enormously [34]. The first systematic measurements of lamellar spacing was done by Mehl and his colleagues [35]. They showed that lamellar spacing decreased as undercooling, ΔT, below the eutectoid temperature increased. Zener analyzed previous spacing measurement in a more theoretical way [2]. He considered a volume of pearlite of depth 'b' and interlamellar spacing 'S' growing towards the x-direction. If the pearlite proceed to the x-direction by $\mathrm{d}x$, then the volume of austenite which is transformed to pearlite is $Sb\rho\mathrm{d}x$, where ρ is the density. The available free energy ΔG to form that volume of pearlite is :

$$\Delta G = \Delta H \left(\frac{T_e - T}{T_e} \right) Sb\rho \, \mathrm{d}x \tag{1}$$

where, T_e is eutectoid temperature, T is transformation temperature, and ΔH is latent heat of transformation. This volume of pearlite transformation leads to an increase in the ferrite/cementite interface energy. The increase in interfacial area will be $2b \, \mathrm{d}x$, and in interface energy will be :

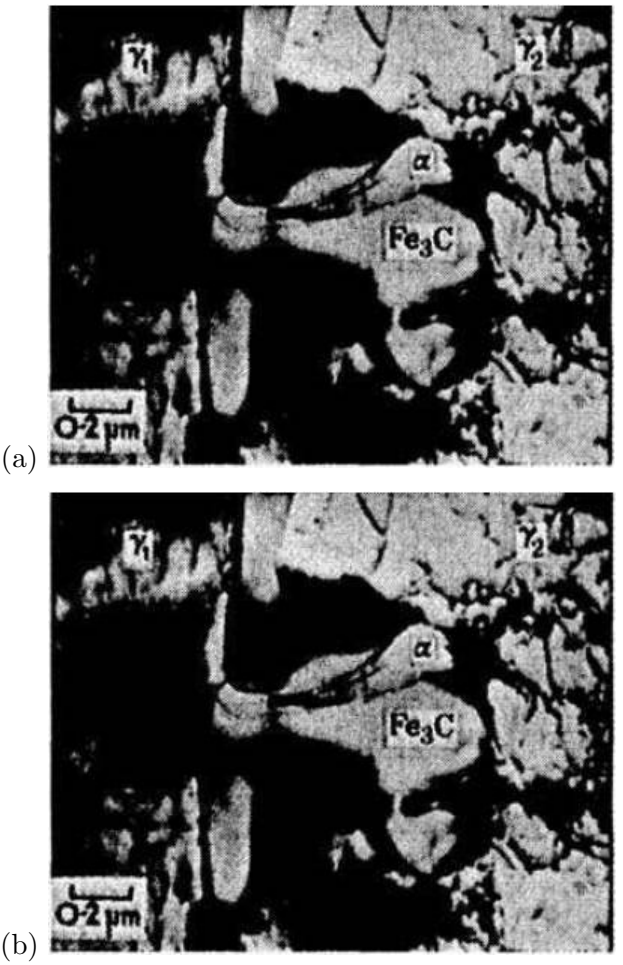

(a)

(b)

Figure 2: Fe-13Mn-0.8C (in wt%) partly transformed at 600°C. austenite is retained in conjunction with ferrite and cementite: (a) nucleation of a pearlite nodule on grain boundary cementite, (b) interface of nodule with austenite. Transmission electron microscopy of thin-foil sample [33].

$$\text{Interfacial energy increase due to transformation} = 2\sigma b \, \mathrm{d}x \tag{2}$$

Pearlite growth can only be possible when surface energy does not exceed total Gibbs free energy in the system. Therefore, the condition for growth can be found from Eq. 1 and 2:

$$\Delta H \left(\frac{T_e - T}{T_e} \right) \rho S = 2\sigma \tag{3}$$

This is a simple treatment that neglects any strain energy term. Moreover, the enthalpy change per unit mass was assumed to have same specific heats of austenite and pearlite. Anyhow, Eq. 3 implies three important views of the pearlite transformation:

1. The lamellar spacing of pearlite S decreases with transformation temperature.

2. Minimum value of interlamellar spacing is decided by total free energy available in the system.

3. There is a linear relationship between reciprocal of transformation temperature and interlamellar spacing.

The interlamellar spacing of pearlite was assumed to have a constant value during the transformation in Zener's previous theoretical analysis. However, it could have fluctuation of the spacing because of impingement between colony, inhomogeneous chemical distribution and the other complex lamellar morphology. The practical measurement of the spacing was criticized in previous reasons. Forced velocity pearlite growth suggested by

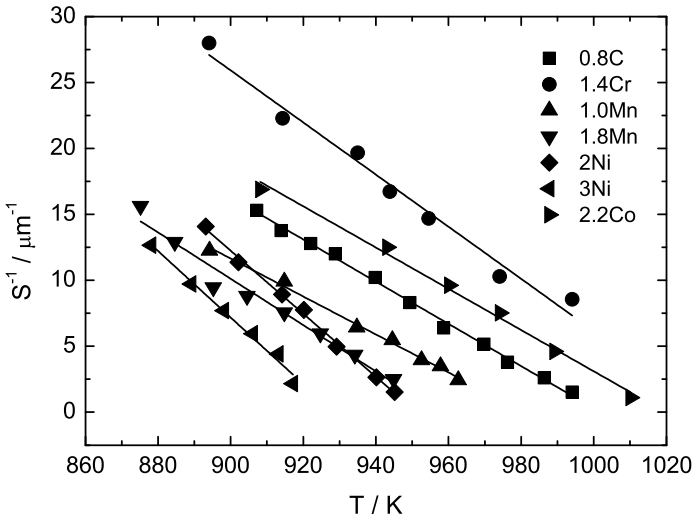

Figure 3: Collected data of T vs reciprocal of interlamellar spacing S [5].

Bolling and Richman [36] is a method that a rod specimen is applied the translating temperature gradient which establishes a single transformation interface which is sufficiently steep to prevent nucleation ahead of the growing front. As a result, pearlite colonies grow with a constant velocity. This technique should be distinguished from isothermally transformed pearlite growth rate measurement with respect to the fact that the growth rate is fixed as imposed by the translation velocity and transformation temperature is a free variable. In the series of experiments by Ridley and his co-workers [5], the pearlite growth rate was measured under conditions of maximum velocity as possible in the system. Therefore, they measured the minimum interlamellar spacing in the observed lamellar structure before pearlite colonies impinged with each other.

In the Fe-C binary system, the spacing does have fluctuation but they were within a certain range because austenite fully decomposes to ferrite and cementite with same average composition. On the other hand, in the Fe-X-C ternary system where X stands for substitutional solute, it is possible that pearlite may not consume all of the system. This happens because the substitutional solute partitioning occurs between the phases so the austenite is enriched or depleted as pearlite grows. This change of austenite composition causes a reduction in the driving force for transformation. Those effects lead to an increase in the spacing as pearlite grows and finally the transformation stops with retained austenite at the transformation temperature. This form of lamellar structure is called "divergent pearlite". Further study for divergent pearlite was done by Hillert [38]. In the Fe-X-C ternary phase diagram, if the mean composition of the system (grey circle in Fig. 2.2) is located in the three phase field ($\alpha + \gamma + \theta$), the two product phases, ferrite (α) and cementite (θ), have composition

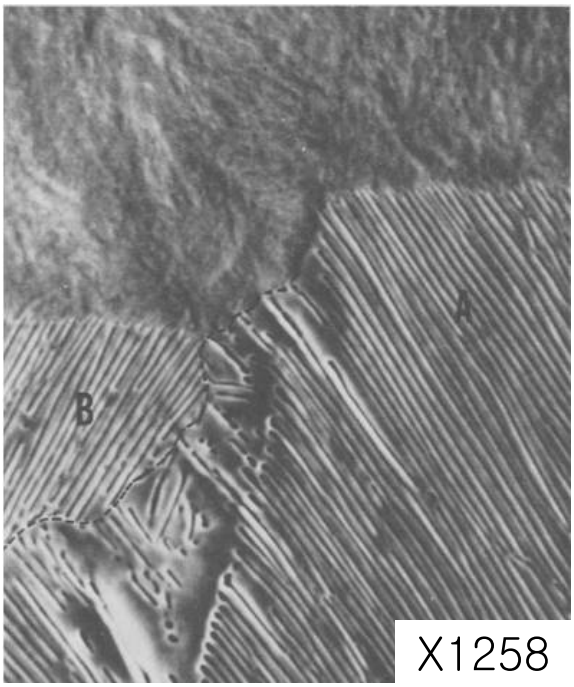

Figure 4: A longitudinal section of forced velocity pearlite at a quenched interface with a prior austenite grain boundary separating pearlite colonies A and B [37].

at point 'a' and 'b'. It is clear that the average composition of pearlite must be fall on the line connecting 'a' and 'b'. Because the average alloy content in austenite and pearlite is maintained constant, pearlite will form with composition at the point noted as a grey square. The growing pearlite represented by the square point will draw carbon from austenite. This causes a carbon-depleted zone of austenite, therefore, the composition of the austenite gradually moves from the mean position to where it meets the critical iso-activity line. This means that the driving force, Δu, which is used for partitioning of alloying element is exhausted. As a result, the pearlite growth rate goes to zero, and interlamellar spacing gradually increases. This phenomenon was first observed by Kuo [39] in the so-called δ-eutectoid reaction in some high-alloy steels. Cahn and Hagel [40] first designated the form "divergent pearlite". Divergent pearlite incompletely transforms austenite when equilibrium is reached between ferrite, austenite and cementite..

2.3 The Crystallography of Pearlite

In a single colony of pearlite, there are only two interpenetrating single crystals of ferrite and of cementite. Neither of α nor θ have an orientation relationship with austenite grain in which they grow. However, there is a clear crystallographic orientation between the ferrite and cementite lamellae in the same pearlite colony. Two orientation relationships have been found during pearlite growth [42]:

- Pitch/Petch relationship
  $(001)_\theta \backslash\backslash (\bar{5}2\bar{1})_\alpha$,
  $(010)_\theta$ $2-3^\circ$ from $[11\bar{3}]_\alpha$,
  $(100)_\theta$ $2-3^\circ$ from $[131]_\alpha$.

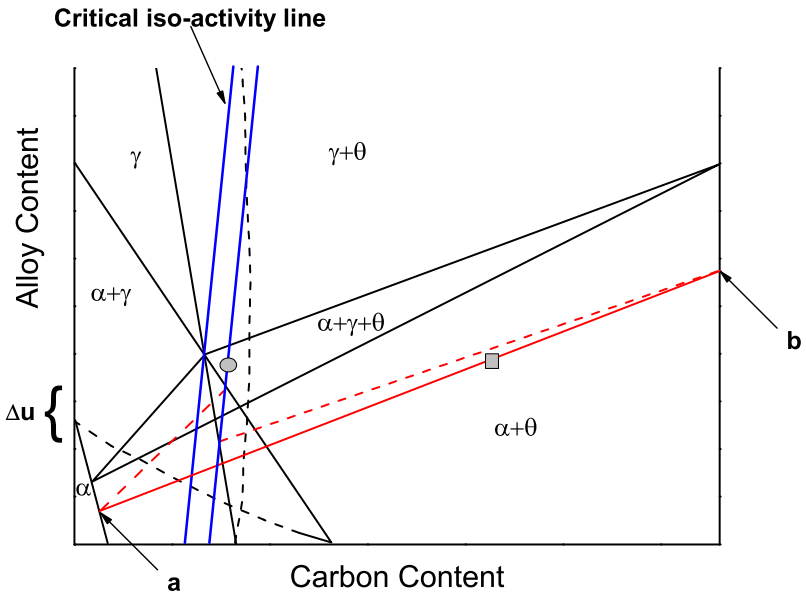

Figure 5: Example of ternary steel phase diagram with steel composition in grey circle.

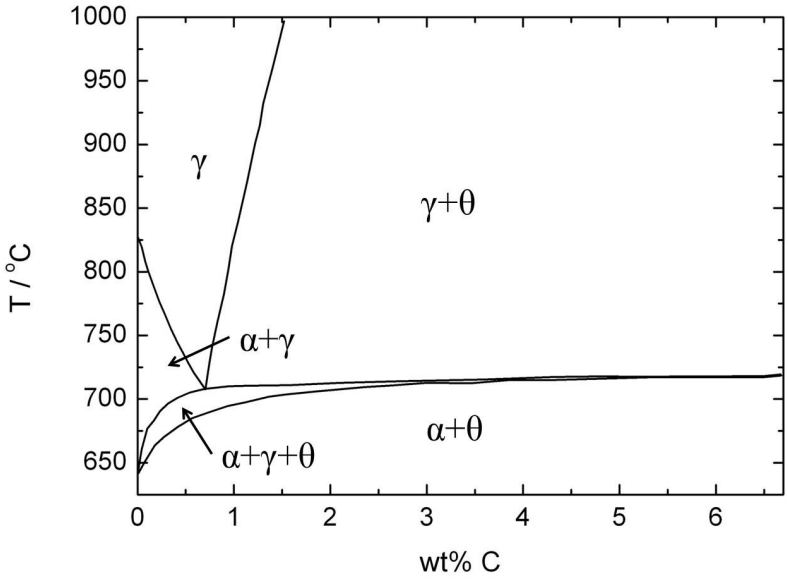

Figure 6: Fe-2Mn-C isoplethal phase diagram calculated using Thermo-Calc with TCFE database [41].

- Bagaryatski relationship
  $(100)_\theta \backslash\backslash (0\bar{1}1)_\alpha$,
  $(010)_\theta \backslash\backslash (1\bar{1}\bar{1})_\alpha$,
  $(001)_\theta \backslash\backslash (211)_\alpha$.

These two relationships are found in the same steel, and the frequency of each relationships is varies rather unpredictably.

2.4 Diffusion Mechanism in Metals

The diffusion of substitutional atoms in metals is controlled by a vacancy mechanism. The diffusivity of substitutional solutes can be written in the classical form:

$$D = ga^2\nu \exp\left(-\frac{\Delta H_{\text{form}} + \Delta H_{\text{m}}}{kT}\right) \exp\left(\frac{\Delta S_{\text{form}} + \Delta S_{\text{m}}}{k}\right) \qquad (4)$$

where g is a geometric factor, a is the lattice constant, ν is an attempt frequency and T is in the absolute temperature. ΔH_{form} and ΔH_{m} are the enthalpy changes associated with the formation and migration of the vacancy respectively, and ΔS_{form} and ΔS_{m} are the corresponding changes in entropy involved with the formation and migration of the vacancy.

Except the enthalpy related term, $\exp\left(-\frac{\Delta H_{\text{form}}+\Delta H_{\text{m}}}{kT}\right)$, the other terms are reduced in one term as a pre-exponential factor, D_0. The activation energy, Q is the summation of $\Delta H_{\text{form}} + \Delta H_{\text{m}}$. The pre-exponential factor was calculated by following the theory of the transition state in the work of Bokshtein [43]. D_0 was predicted in range 10^{-2} and $1\,\text{cm}^2\,\text{s}^{-1}$ and

lower values than these are incompatible.

The concentration of vacancies in the material increases exponentially with temperature. However, the concentration is not large, for example, it does not exceed 0.01-0.1 vol.% near the melting temperature.

2.4.1 Volume diffusion of carbon in austenite

The volume diffusion coefficient of carbon in austenite depends strongly on carbon concentration. The dependence on concentration makes more kinetic analysis more difficult of various diffusion-controlled reactions that arise in steels. Ågren gave an analytical approximation to the diffusion coefficient of carbon in austenite lattice [44]:

$$\begin{aligned} D_{\mathrm{C}}^{\gamma} =& 4.53 \times 10^{-7}\big(1 + Y_{\mathrm{C}}(1 - Y_{\mathrm{C}})\frac{8339.9}{T}\big) \\ & \times \exp\big\{ -(\frac{1}{T} - 2.221 \times 10^{-4})(17767 - 26436 Y_{\mathrm{C}})\big\} \end{aligned} \tag{5}$$

where D_{C}^{γ} is volume diffusion coefficient of carbon in austenite (in $\mathrm{m^2\,s^{-1}}$) and T is temperature in K. Y_{C} is the site fraction of carbon in the interstitial sub-lattice is given by:

$$Y_{\mathrm{C}} = \frac{x_{\mathrm{C}}}{1 - x_{\mathrm{C}}} \tag{6}$$

where x_C is the mole fraction of carbon in the steel.

During the transformation, the existence of substantial carbon concentration gradients at the growth front should account for the variation of D_{C}^{γ} with x_{C}. Trivedi and Pound [45] demonstrated that a weighted average diffusivity $\bar{D}$ can adequately represent the effective diffusivity of carbon that

is needed for the application of the theory of diffusion-controlled growth. They obtained:

$$\bar{D} = \int_{c_\gamma^{\gamma\alpha}}^{\bar{c}} \frac{D\{c^\gamma, T\}}{\bar{c} - c_\gamma^{\gamma\alpha}} \mathrm{d}x \tag{7}$$

where $\bar{c}$ is the average carbon content of the alloy and $c_\gamma^{\gamma\alpha}$ is the maximum permissible carbon content in the austenite at the transformation interface. c_γ is mole fraction of carbon in austenite.

It is necessary to determine experimentally $D\{c^\gamma, T\}$ at least in the range of $\bar{c}$ and $c_\gamma^{\gamma\alpha}$. Kaufman *et al.* [46] tried to overcome this problem by assuming an activation energy of volume diffusion of carbon in austenite. The pre-exponential factor of diffusivity was extrapolated beyond the range of experimental observations.

Bhadashia [47] used the method suggested by Siller and McLellan [48]. The method makes no assumption about the activation energy, the extrapolation which are mentioned above, but it used a general expression for $D\{c^\gamma, T\}$, where T is absolute temperature. The method has two important factors that should be taken account for the modelling of $D\{c^\gamma, T\}$, one is the concentration dependence of the activity of carbon in austenite [49], and secondly, the repulsive interaction between nearest neighbouring carbon atom located in octahedral sites [50].

The equation of Siller and McLellan described $D\{c^\gamma, T\}$ using their terminology, as follows:

$$D\{c^\gamma, T\} = D'\xi\{\theta\} \tag{8}$$

where θ is the atomic fraction of carbon and D' is a temperature dependent but carbon concentration independent term. D' is set by using absolute reaction theory [51] expressed as:

$$D' = \frac{kT}{h} \exp\left(- \frac{\Delta G^a}{kT} \right) \left(\frac{\lambda^2}{3\gamma_m} \right) \tag{9}$$

where k is the Boltzmann constant, h is Planck constant, γ_m means activity coefficient of the activated complex, assumed constant and λ is distance between the $\{002\}$ austenite planes. The ΔG^a is an activation free energy which is independent of composition and temperature, and represents the difference in free energy between the 'activated complex' and the 'reactants' when each is in its standard state at the temperature of 'reaction'. Using a first order quasi chemical thermodynamic model [50] for carbon in austenite combined with reaction rate theory, Siller and McLallan showed that the concentration dependent part of Eq. 8 or $\xi\{\theta\}$ is given by:

$$\xi\{\theta\} = \alpha \left(1 + \frac{z(1+\theta)}{1 - \left(\frac{z}{2}+1\right)\theta + \frac{z}{2}\left(\frac{z}{2}+1\right)(1-\sigma)\theta^2} \right) + (1+\theta)\frac{\mathrm{d}\alpha}{\mathrm{d}\theta} \tag{10}$$

where, z is the coordination number of octahedral interstitial site in the austenite lattice, α is the activity of carbon, and σ is expressed as:

$$\sigma = 1 - \exp\left(- \frac{\Delta\epsilon}{kT} \right) \tag{11}$$

where $\Delta\epsilon$ is the energy due to the repulsive interaction between neighbouring carbon atoms, taken to be $8235\,\mathrm{J\,mol^{-1}}$. In the work of Bhadeshia, it was found that $\Delta G^a/k = 21230\,\mathrm{K^{-1}}$ and $\ln(3\gamma_m/\lambda^2) = 31.84$ [47].

2.4.2 Grain boundary diffusion

A grain boundary (GB) has an important role as a diffusion short circuit, for example, in sintering, diffusion-induced grain boundary migration, discontinuous reactions (such as discontinuous precipitation, discontinuous coarsening, etc.), recrystallisation, and grain growth. GB diffusion not only has an effect at high temperatures but also is particularly significant at low, and even ambient temperatures.

The first direct observation of GB diffusion was made using autoradiography in 1950 [52]. This was follwed in 1951 by Le Claire [53] gave additional blackening of autoradiographic images along grain boundaries indicated that the radio tracer atoms penetrated into grain boundaries much faster than in regular lattice.

In the work of Fridberg *et al.* [54], the GB self-diffusion coefficient of iron have similar behaviour in ferrite and austenite. It implies that GB diffusion is almost independent of lattice structure. Moreover, Fridberg figured out that the GB diffusion coefficients of Cr, Mn, Ni and Mo have nearly same GB diffusion coefficient with self-diffusion of iron in GB. This fact is predictable because they are the nearest neighbours of iron in the periodic table. The measured GB self-diffusion coefficient of iron, δD_B in Fridberg's work is:

$$\delta D_B = 5.4 \times 10^{-14} \exp\left(- \frac{155000\,\mathrm{J\,mol^{-1}}}{RT} \right) \quad \mathrm{m^3\,s^{-1}} \tag{12}$$

2.5 Growth Mechanisms of Pearlite

Three mechanisms have been suggested for pearlite growth. Those mechanisms can be distinguished by the diffusion paths of solute in decomposing austenite. One is that solute atoms diffuse through the austenite lattice during redistribution. The transformation front is also considered as diffusion short circuit like grain boundary does in another mechanism. However, if two possible diffusion paths exists, they should be considered at the same during the transformation. Therefore, the other, mixed-diffusion mechanism, accounts for both volume and boundary fluxes.

2.5.1 Volume diffusion mechanism

For any diffusional transformation, solute atoms should be redistributed. In pearlite growth, carbon is transported from the edges of ferrite lamellae to neighbouring cemcentite lamellae [3]. The volume diffusion mechanism assumes that the carbon diffuse through the parent austenite. Let's assume that the interfaces of ferrite-cementite, ferrite-austenite and cementite-austenite are planar, then, the concentration difference that drives the diffusion would be $(c^{\gamma\alpha} - c^{\gamma\theta})$, where $c^{\gamma\alpha}$ and $c^{\gamma\theta}$ are the concentrations in austenite which is in equilibrium with ferrite and cementite respectively. Those interface compositions in ferrite and cementite can be obtained from the extrapolated phase boundaries, $\alpha/\alpha+\gamma$ and $\gamma/\gamma+\theta$ of the Fe-C phase diagram. However, phase boundaries are not linear but have a thermodynamic basis. Thus, the extrapolation should be based on thermodynamic considerations. At the pearlite growth front, the actual concentration difference is approximately $(1 - S_C/S)(c^{\gamma\alpha} - c^{\gamma\theta})$ because of interface energy between ferrite and cementite in pearlite [2]. Zener suggested this analysis where S_C is the critical interlamellar spacing. The term $(1 - S_C/S)$ ac-

counts the decreased fraction of total free energy for assembling interfaces between ferrite and cementite. In other words, it is the ratio of free energy for diffusion of solute to total amount of available free energy in the system. The term $(1 - S_C/S)$ was derived in the work of Hillert [8]. The molar free energy for making the α/θ interface, $\Delta G_m^{\text{interface}}$, without the part of energy for transformation can be described as:

$$\Delta G_m^{\text{interface}} = \frac{2\sigma^{\alpha\theta} V_m}{S} \tag{13}$$

where $\sigma^{\alpha\theta}$ is α/θ interfacial energy per unit area and V_m is the molar volume of austenite. If the interlamellar spacing, S, decreases and reaches S_C, the free energy consumed by interfaces would have same value as the total free energy of the system and pearlite growth should stop because there is no available energy for transformation. Thus,

$$\Delta G_m^{\text{total}} = \frac{2\sigma^{\alpha\theta} V_m}{S_C} \tag{14}$$

where $\Delta G_m^{\text{total}}$ is total free energy available in the system. As a result, the free energy is reduced by factor of $(\Delta G_m^{\text{total}} - \Delta G_m^{\text{interface}})/\Delta G_m^{\text{total}} = (1 - S_C/S)$. The diffusional flux of carbon from the edge of a ferrite to a neighbouring cementite lamellae can be written as [8]:

$$J = -\frac{A^\alpha}{V_m} D_{\text{C}}^\gamma \frac{\mathrm{d}c}{\mathrm{d}x} = \frac{D_{\text{C}}^\gamma b S^\alpha}{V_m} \frac{(c^{\gamma\alpha} - c^{\gamma\theta})}{S^\alpha/2} \tag{15}$$

where, J is a flux, molar volume V_m is considered same for all the related phases with pearlite transformation, A^α is the cross sectional area of the interface, which is equal to bS^α, b is an arbitrary distance perpendicular to the growth direction. The diffusion distance can be approximated to $S^\alpha/2$

for the growth of ferrite lamellae. This diffusion flux causes the edgewise growth of ferrite lamellae in austenite with a growth rate, v and can be represented as:

$$J = \frac{vbS^{\alpha}}{V_m}(\bar{c} - c^{\alpha\gamma}) \tag{16}$$

where $\bar{c}$ is the mean composition of the system or austenite far from the growth interface. The volume fraction between phases or thickness ratio of α and θ in pearlite is calculated from the lever rule with the composition, $c^{\alpha\gamma}$, $c^{\theta\gamma}$, and $\bar{c}$. After neglecting volume change which accompanies the reaction, the material balance at the tip of each lamellae is given by:

$$\frac{vbS^{\alpha}}{V_m}(\bar{c} - c^{\alpha\gamma}) = \frac{vbS^{\theta}}{V_m}(c^{\theta\gamma} - \bar{c}) = \frac{vbS^{\alpha}S^{\theta}}{SV_m}(c^{\theta\gamma} - c^{\alpha\gamma}) \tag{17}$$

where S^{α} and S^{θ} are the thickness of each ferrite and cementite lamellae respectively and S is a interlamellar spacing. Equating equations 16 and 17, we get:

$$v = \frac{2D_{\mathrm{C}}^{\gamma}S}{S^{\alpha}S^{\theta}}\left(\frac{c^{\gamma\alpha} - c^{\gamma\theta}}{c^{\theta\gamma} - c^{\alpha\gamma}}\right) = \frac{2D_{\mathrm{C}}^{\gamma}S}{S^{\alpha}S^{\theta}}\left(\frac{c_e^{\gamma\alpha} - c_e^{\gamma\theta}}{c^{\theta\gamma} - c^{\alpha\gamma}}\right)\left(1 - \frac{S_C}{S}\right) \tag{18}$$

where $c^{\alpha\gamma}$ is the composition of ferrite at the α/θ interface, and the other terms like this have similar meaning.

Ridley suggested a simpler form of the pearlite growth rate equation based on the relation between growth rate, spacings, concentration gradient and diffusivity [5]. In Ridley's work, it was assumed that the concentration difference is proportional to amount of undercooling, which in turn is proportional to reciprocal spacing. Therefore, the growth rate equation for

volume diffusion mechanism of pearlite can be written as:

$$vS^2 = k_1 D \tag{19}$$

where k_1 is thermodynamic term which roughly constant. The Zener-Hillert method has been used for rate controlling factor of pearlite growth. The usual method for calculating equation 18 was to incorporate the measured values of interlamellar spacings, calculated interfacial compositions and the diffusion coefficient into the equation and then compare the calculated growth rates with those determined experimentally. Many researchers have believed that the volume diffusion mechanism of pearlite growth is a reasonable rate controlling step, even though there was a discrepancy of up to 50 times or more.

Bramfitt and Marder [55] used forced velocity growth to study pearlite for Fe-C alloys at the first time. Bolling and Richman [36] used this technique to examine the relation vS^n = constant, where $n = 2.3 \pm 0.1$, and this is another rough assumption for equation 18. Another forced growth experiment by Verhoeven and Pearson [56] measured the exponent n to 2.07. For many other similar experiments has gave the result close to vS^2 = constant and seemed to be good proof for volume diffusion being the rate controlling factor. The forced velocity pearlite growth can give uniform colonies with constant interlamellar spacing, however, in the context of avoiding impingement, it has limitations when used to measure the growth rate of pearlite.

There have been many attempts to calculate the pearlite growth rate using volume diffusion of carbon as the rate controlling factor. However, there still important exist discrepancies with the experimental results. When

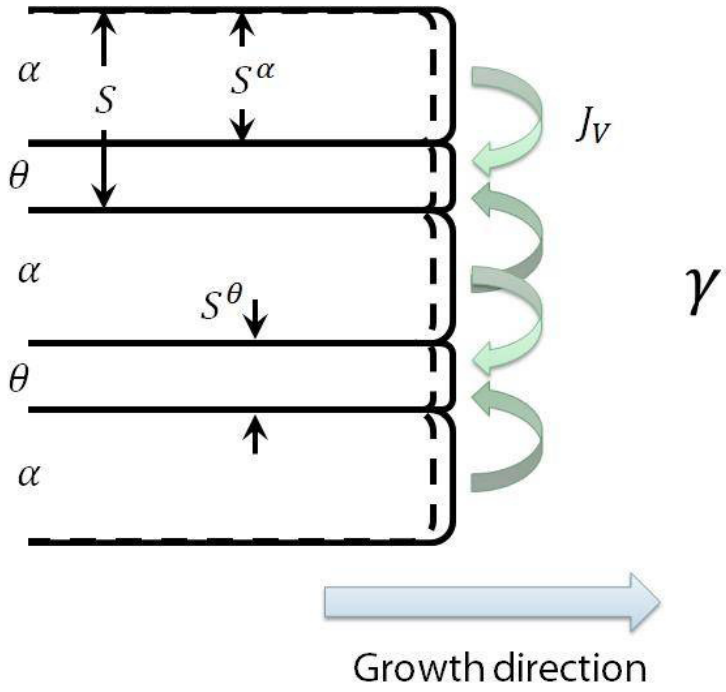

Figure 7: Schematic diagram of volume diffusion controlled growth of pearlite.

it applied to a ternary system [57], there are severe inconsistencies with growth at low temperatures, attempts were made to introduce boundary diffusion model.

2.5.2 Boundary (or interface) diffusion mechanism

As the volume diffusion mechanism is not sufficient to explaining pearlite growth, the researchers tried to introduce alternative diffusion path, the

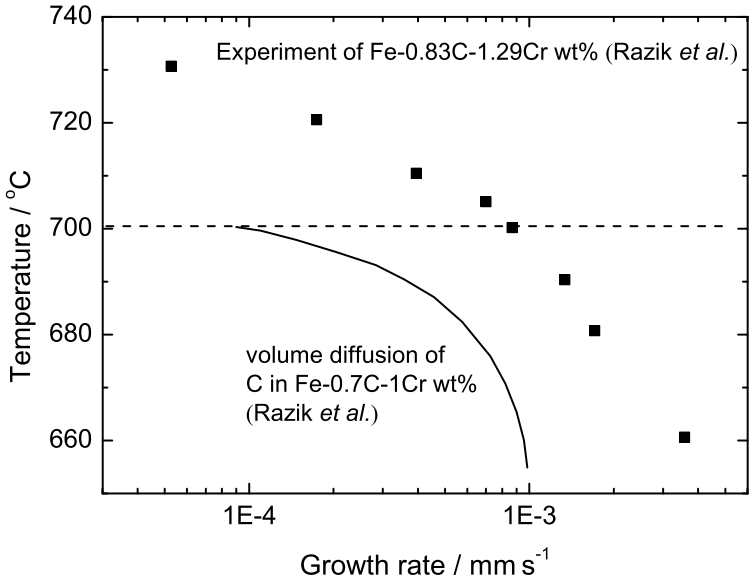

Figure 8: Calculated growth rate based on volume diffusion mechanism shows underestimation of experimental results.

boundary between pearlite and austenite. Boundary diffusion has been known to have faster diffusivity and lower activation energy than volume diffusion in Fe-C and other non-ferrous alloys. Cahn and Hagel [40] suggested that boundary diffusion is the most plausible explanation for growth mechanism of pearlite. Sundquist tried to apply the boundary diffusion as a dominant mechanism for driving the edgewise growth of pearlite [7]. In the work of Sundquist, local equilibrium and effect of capillarity were accounted for modelling. The activation energy of surface diffusion coefficient was deduced from the experimental results of Fe-C steels. The value was $191\,\mathrm{kJ\,mol^{-1}}$ which was far too higher than that of volume diffusion of carbon in austenite. Although, it could be affected by the presence of impurity atoms in steel, the justification seems to be unrealistic.

Hillert modified Zener-Hillert volume diffusion mechanism for the boundary diffusion controlled growth [8]. Hillert slightly modified the equation 15 that the cross sectional area takes place to be equal to $2b\delta$, where, δ is the thickness of the boundary layer. The factor of 2 exists for the diffusion on both sides of ferrite lamellae. The diffusion distance $\mathrm{d}x$ was taken proportional to S to make the result independent of ferrite and cementite and was approximated to $S/4$ for the case of symmetric eutectoid.

The flux of solute through the boundary between austenite and pearlite can be represented as:

$$J = -\frac{A^{\alpha}}{V_m} D_B^{\mathrm{C}} \frac{\mathrm{d}c}{\mathrm{d}x} = \frac{2D_B^{\mathrm{C}} b\delta}{V_m} \frac{(c^{\gamma\alpha} - c^{\gamma\theta})}{S^{\alpha}/4} \tag{20}$$

where D_B^{C} is the boundary diffusion coefficient of carbon. As in the previous section, the mass flow causes both the phases to grow and their growth rate

must be equal. Assuming there are no volume changes during the austenite to pearlite reaction and considering the material balance at the edges of ferrite and cementite lamellae, the lever rule can be used to relate the lamellar thickness with the growth rate as in equation 17.
Combining equation 17 and equation 20 results in:

$$v_B = \frac{8D_B^{\mathrm{C}}\delta}{S^{\alpha}S^{\theta}}\left(\frac{c_e^{\gamma\alpha} - c_e^{\gamma\theta}}{c^{\theta\gamma} - c^{\alpha\gamma}}\right)\left(1 - \frac{S_C}{S}\right) \tag{21}$$

Turnbull suggested that boundary diffusion is one of the important parameters has effect on the precipitation rate, and the rate of cell growth in this theory of cellular precipitation [58]. He described that the cell boundary (or interface) provides a diffusion short circuit for the solute atoms. This cell boundary is incoherent and sweeps all of solutes as cell grows in diffusional transformation. Seith and Laird [59] report that the boundary diffusion cause many orders of magnitude greater growth rate in precipitation of tin from lead compares to those calculated from the diffusion data assuming volume diffusion mechanism. In the tin precipitation, if the solute is drained only by diffusion along the cell boundary during the cell growth, the growth rate will follow:

$$v_B = \left(\frac{c_e^{\gamma\alpha} - c_{\infty}^{\gamma}}{c^{\gamma\alpha}}\right)\left(\frac{\delta}{\tau_1}\right) \tag{22}$$

where c_{∞}^{γ} is parent phase composition at far away from the cell boundary, and τ_1 is the time required to drain the solute from the grain boundary region and is given by:

$$\tau_1 = \frac{S^2}{D_B} \tag{23}$$

where D_B is diffusion coefficient of tin in the cell boundary. Therefore,

$$v_B = \left(\frac{c_e^{\gamma\alpha} - c_\infty^{\gamma}}{c^{\gamma\alpha}}\right)\left(\frac{\delta D_B}{S^2}\right) \tag{24}$$

According to Turnbull's analysis, the observed growth rate in Seith and Laird [59] leads to the D_B have to be 10^{-6} to $10^{-7}\,\mathrm{cm^2\,s^{-1}}$. Assuming the Langmuir-Dushman equation is applicable, this magnitude of D_B correspond to an activation energy, Q_B, for boundary diffusion equals to $37.68\,\mathrm{kJ\,mol^{-1}}$, compared with the activation energy of volume diffusion, Q_V which is $108.7\,\mathrm{kJ\,mol^{-1}}$. The ratio Q_B/Q_V is 0.35 and agrees fairly well with $Q_B/Q_V = 0.44$ for self-diffusion in silver. This was thought to be reasonably sound evidence to justify that the diffusion of tin atoms along the cell boundary was the rate controlling factor since it was entirely consistent with experimental results.

For more than ternary alloying system, the partitioning of substitutional element, X, is becoming significant during the pearlite growth. It seems to make sense that boundary diffusion of X has more important role as a rate controlling mechanism in this case. The volume diffusion coefficient of substitutional alloying element is much smaller than that of carbon. Thus, the boundary between pearlite and parent austenite would provide the diffusion short circuit for substitutional alloying element and partition into the product phases [3]. The boundary diffusion controlled growth rate, v_B can be written as:

$$v_B = \frac{12 s D_B^{\mathrm{X}} \delta S^2}{S^\alpha S^\theta}\left(\frac{c_{\mathrm{X}}^{\gamma\alpha} - c_{\mathrm{X}}^{\gamma\theta}}{c_{\mathrm{X}}^{\theta\gamma} - c_{\mathrm{X}}^{\alpha\gamma}}\right)\frac{1}{S}\left(1 - \frac{S_C}{S}\right) \tag{25}$$

where the boundary segregation coefficient, s, is the ratio between alloying

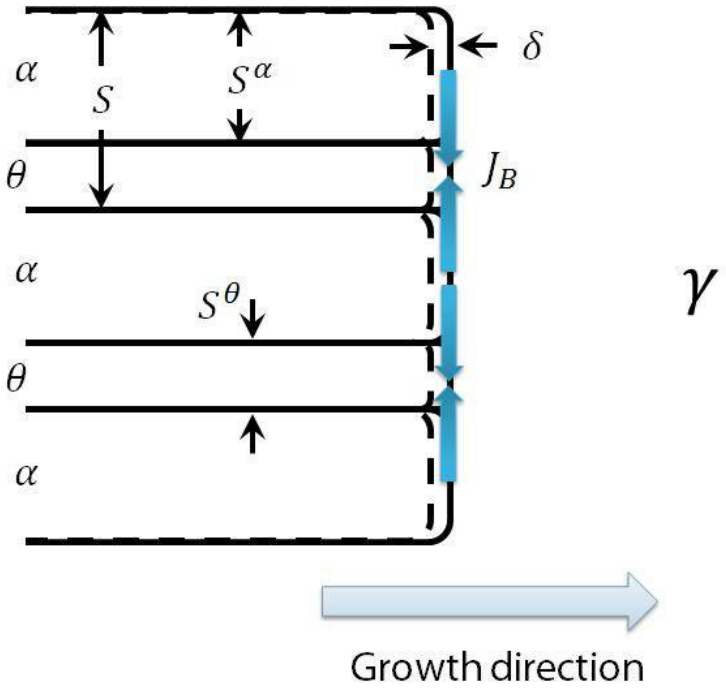

Figure 9: Schematic diagram of pearlite which grows with boundary diffusion mechanism.

element concentration in austenite near the boundary and at the boundary, $c_{\mathrm{X}}^{\gamma\alpha}$ and $c_{\mathrm{X}}^{\gamma\theta}$ are the concentrations of X in austenite which is equilibrium with ferrite and cementite and $c_{\mathrm{X}}^{\alpha\gamma}$ and $c_{\mathrm{X}}^{\theta\gamma}$ are ferrite and cementite concentration of X which is equilibrium with austenite respectively. s is assumed as value 1 because the pearlite/austenite boundary is moving, therefore, there is no time for segregation.

2.5.3 Other suggested pearlite growth mechanisms

In the work of Cahn and Hagel [40], The diffusion process of both interstitial and substitutional solutes was considered to use the diffusion path in austenite, ferrite and along the austenite-pearlite interface. Because there is considerable difference of opinion about the exact growth mechanism of pearlite, they took a different approach rather than calculating the growth rate of pearlite based on any of previous mechanisms. They tried to check the consistency between the measured growth rate, interlamellar spacing and the diffusion coefficients.

Cahn and Hagel suggested a kinetic parameter β_i, which gave a measure of resistance to segregation. There exists only one parameter for each element and each phase.

$$\beta_i = \frac{vS}{2\pi D_i^V} \tag{26}$$

Another term β_i' can be written in terms of the thermodynamic parameter:

$$\beta_i' = \frac{1}{2}\frac{c_i^{\gamma\alpha} - c_i^{\gamma\theta}}{c_i^{\theta\gamma} - c_i^{\alpha\gamma}} \tag{27}$$

where $c_i^{\gamma\alpha}$, $c_i^{\gamma\theta}$, $c_i^{\theta\gamma}$ and $c_i^{\alpha\gamma}$ are the concentration which can be obtained from the phase diagram and i represents the carbon or substitutional solute. If β_i is large (for example, low D_i^V, high v or high S) and since there is an upper limit to $(c_i^{\gamma\alpha} - c_i^{\gamma\theta})$, $(c_i^{\theta\gamma} - c_i^{\alpha\gamma})$ will be small and hence little partitioning of solute element, i will occur. When β_i is small (*i.e.* high D_i^V, high v or high S), because there is an upper limit to $(c_i^{\theta\gamma} - c_i^{\alpha\gamma})$, $(c_i^{\gamma\alpha} - c_i^{\gamma\theta})$ will be small and hence the concentration gradient driving the diffusion at the pearlite-austenite interface would be small. β_i can be calculated from ex-

perimental data (D_i^V, v and S) with equation 26 and β_i' can be established from phase diagram. For Fe-C binary system, it is possible to calculate the upper limit of $(c_i^{\gamma\alpha} - c_i^{\gamma\theta})$ and a lower limit of $(c_i^{\theta\gamma} - c_i^{\alpha\gamma})$. Because the carbon concentration in cementite can not be zero, thus the upper limit of β_i' based on equation 27 would be half their ratio and this is termed as β_0. For comparing β_0 and β_i, Cahn and Hagel calculated β_0 from phase diagram and β_i based on experimentally reported v and S. They suggested that the opinion that the value of D_i^V which make $\beta_i = \beta_0$ or denoted as apparent diffusivity, D_{app}, would be necessary to satisfy the required segregation of solute atoms.

If the value of β_i is equal to that of β_0, then it can be strong proof for volume diffusion of solute in austenite is rate controlling factor of the pearlite growth. On the other hand, if the β_i is less than β_0, then some process other than the diffusion in austenite is controlling the rate. If the β_i is larger than β_0, this can be strong proof for the existence of a faster diffusion path.

In the case of non-ferrous pearlite, Cahn and Hagel showed that the apparent diffusion coefficients, D_{app}, are higher than D_i, which are measured from experiments, by orders of magnitude. Therefore, β_i is larger than β_0 and it can be considered as strong indication that there is alternative diffusion path or diffusion short circuit. For the pearlite in Fe-C binary steels, D_i and D_{app} seems to have good agreement in a reasonable range for which the v, S and β_0 are known. Hence, the carbon diffusion in austenite can be considered as the main rate controlling factor. However, in that work, the v and S that they used in their calculation were not measured for same steel. Moreover, in Fe-C binary system, the pearlite growth rate is limited

by the range of carbon diffusion in austenite allows, but in their report, high purity steels shows almost 50 times faster pearlite growth rate than plain carbon steel. This could well be attributed to the spacings in high purity steels, but the measurements showed that the spacings were almost comparable to those in plain carbon steels. this further strengthens the fact that another mechanism is operative for carbon diffusion.

Diffusion through ferrite in pearlite colony was also considered by Nakajima *et al.*. [12] and Pandit and Bhadeshia [10]. Nakajima and his colleagues analyse this matter first using a phase field approach. They reported that since diffusion in ferrite is much faster than that in austenite and when this was simultaneously active with volume diffusion in austenite, the difference in calculated and the experimental growth rate of pearlite was narrowed down. They argued that the flux through both austenite and ferrite results more faster growth rate compared to the one flux through austenite and the reason why was due to a large ratio of ferrite-cementite interfacial area as compared to that in case of cementite-austenite interfaces. The phase field calculations that they were used showed the thickening of cementite behind the transformation front when the diffusion occurs in ferrite. Cahn and Hagel considered the effect of volume diffusion in ferrite, but they did not observed any tapering of cementite at the transformation front. Since the calculated velocities were still not able to explain the observed growth rates, they attributed the same to the influence of transformation strain or diffusion through the boundary. Phase field modelling which consider transformation strain and diffusion in austenite and ferrite was done by Steinbach and Apel [60]. In their report, they figured out that the transformation strains inhibit the co-operative growth of ferrite and cementite resulting in solitary growth of wedge-shaped cementite ahead of the ferrite

which they termed as 'staggered growth'. But in the Fe-C alloys studied to date, wedge-shaped cementite lamellae behind the transformation front has never been observed experimentally. Although the phase field calculations reduced the gap between the calculated and the observed growth rate in Fe-C system, this was fundamentally weak due to the neglect of the mechanism of reconstructive transformation. Thus the transformation strains are mitigated during the reaction due to the flow of iron. It is noticeable that in the previous two reports, the effect of boundary diffusion was ignored due to the lack of boundary diffusion data.

The combination of volume and boundary diffusion was considered by Hashiguchi and Kirkaldy for the first time in Fe-C alloys [9]. They assumed existence of local equilibrium across the transformation front, both of mass flow through the volume of austenite and the advancing pearlite-austenite boundary with a mechanical equilibrium at the interface junction and the effects of capillarity. The boundary diffusion coefficient of carbon was extracted from the experimental growth and spacing data of Brown and Ridley [61]. In their model, the activation energy for the boundary diffusion of carbon was $170\,\mathrm{kJ\,mol^{-1}}$. However, this clearly does not make sense, because the deduced boundary diffusivity has greater activation energy than volume diffusion of both ferrite and austenite. Their theory was too complex to be implemented, requiring approximations which rendered the details unimportant.

Another form of mixed-diffusion model which accounts both boundary and volume flux was suggested by Pandit and Bhadeshia [10]. In their report, they used the flux equations which are derived by Zener and Hillert, the equation 18 and 25. The theory accounts only for the effect of diffusion

fluxes and local equilibrium across the advancing phase boundary unlike Hashiguchi and Kirkaldy. They also extracted the boundary diffusivity of carbon from Brown and Ridley [61] and earn the activation energy which has value $96\,\mathrm{kJ\,mol^{-1}}$. The result shows reasonable value of the activation energy for carbon boundary diffusion, but during the extraction of boundary diffusivity, they used only part of the temperature range in the growth and spacing data of Brown and Ridley. Thus, the data were selected on purpose. Moreover, the interface energy between ferrite and cementite, $\sigma^{\alpha\theta}$ was also calculated from equation 13 and 14 but the value was too large.

2.6 Pearlite in Multicomponent Steels

Almost all of commercialised steel products have more than one alloying element except carbon. The alloying elements in addition to carbon are added for strength, hardenability, toughness and many other reasons. They can be categorised as interstitial and substitutional. They can be distinguished with whether alloyed atom take place the one of lattice position instead of iron atom or locate in the site between the space of crystal. The existence of substitutional alloying atom in the system makes the calculation of diffusion controlled transformation in such systems quite complicated because of the interaction between the alloying element and carbon. The growth of proeutectoid ferrite from austenite in Fe-C-X system, where X is the substitutional alloying element has been studied in considerable details owing to the relative simplicity of the influence of a ternary addition on the growth rate [62, 63]. However, the pearlite growth is more complicated than the growth of proeutectoid ferrite because both growth of ferrite and cementite work in concert during the pearlite transformation and the partitioning behaviour is different. Also, the diffusion path should be considered

for substitutional solute. Pearlite growth rate can be controlled by diffusion of carbon or substitutional solute through the volume of austenite or the pearlite-austenite boundary or simultaneous diffusion of both solutes.

2.6.1 Thermodynamics of ternary systems

In a Fe-C binary system, the tie-line at certain temperature between ferrite-austenite and cementite-austenite uniquely exists. As the figure describes, the tie-line between two phases can be decided by a common tangent construction using a free energy composition diagram and it give the composition of the growing phase (or phases) in equilibrium with the parent phase. However, alloying substitutional solute, X, causes the complication for finding the acting tie-line during the reaction. Now, the free energy curves for the parent and product phases become three dimensional surfaces and an infinite number of tangent planes can be constructed. To decide the acting tie-line in $\alpha+\gamma$ and $\gamma+\theta$ phase field, the two fluxes of carbon and X must be simultaneously satisfied.

$$(c_{\mathrm{C}}^{\gamma\alpha} - c_{\mathrm{C}}^{\gamma\theta})v = -D_{\mathrm{C}}\nabla c_{\mathrm{C}} \tag{28}$$

$$(c_{\mathrm{X}}^{\gamma\alpha} - c_{\mathrm{X}}^{\gamma\theta})v = -D_{\mathrm{X}}\nabla c_{\mathrm{X}} \tag{29}$$

Where the ∇c_{C} is carbon composition gradient at the pearlite/austenite interface, and ∇c_{X} stands for similar meaning to previous notation but gradient of X composition. For the volume diffusion of both X and C in austenite, diffusivity of carbon is 6 orders larger than that of X, or$D_{\mathrm{C}}^{\gamma} \gg D_{\mathrm{X}}^{\gamma}$. Thus the two equations cannot be simultaneously solved using the tie-line passing through the alloy composition. To resolve this issue, Kirkaldy [64] and Purdy *et al.* [17] suggested that the fast diffuser (C) has to slow down and

keep pace with the slow diffusing atom (X) in which case the diffusion driving force for C has to be negligible or the slow diffusing species has to have a large driving force. This is termed as partitioning local equilibrium (PLE) where the alloying element, X, is partitioning between austenite and the product phases. Therefore, the growth rate or reaction rate is slowed down because of the slow diffusivity of the substitutional solute. In another case, it could be possible to consider when the substitutional element is involved in a shot range diffusion (a sharp spike at the interface) and the reaction proceeds by the diffusion of carbon through a combination of austenite. This is termed as negligible partitioning local equilibrium (NPLE) and alloying element affects the reaction kinetics only through its thermodynamic influence on the driving force for carbon diffusion.

In the papers published by Coates [62, 63], it was considered that when the diffusivity difference between two solutes is not only $D_{\mathrm{C}}^{\gamma} \gg D_{\mathrm{X}}^{\gamma}$, but also in various range. Consider a ternary system with component $i = 1, 2, 3$ where 1 and 2 are independent solute and 3 is solvent. At temperature T_1, a specimens of uniform composition $(\bar{C}_1, \bar{C}_2)$ is in a single γ phase field. This alloy undergoes an instantaneous quenching to temperature T_0 then, the composition $(\bar{C}_1, \bar{C}_2)$ located in $\alpha + \gamma$ phase field. To solve the diffusional growth of α precipitate particles in the γ matrix, the following assumptions are made:

1. The diffusion fields around the various precipitate particles do not impinge. This is equivalent to considering the growth of a single particle in an infinite medium of initial composition, $(\bar{C}_1, \bar{C}_2)$.

2. Ternary diffusional interactions are ignored. That is to say, in the

flux equations,

$$J_i = -D_{i1}\nabla C_1 - D_{i2}\nabla C_2 \ (i = 1, 2) \tag{30}$$

the terms $D_{12}\nabla C_2$ and $D_{21}\nabla C_1$ are assumed to be negligible with respect to $D_{11}\nabla C_1$ and $D_{22}\nabla C_2$. In other words, the diffusion field of component 1 does not interact with that of component 2.

Accordingly, these fields are solutions of the binary equation

$$\frac{\partial C_i}{\partial t} = D_i \nabla^2 C_i \tag{31}$$

where it is assumed the diffusion coefficients D_1 and D_2 are not functions of concentration. Although unlike the binary case, the two solute equations are coupled. The effect of capillarity and interface reaction kinetics can be ignored. Therefore, the composition of the precipitate and matrix at the interface, $(C_1^{\alpha\gamma}, C_2^{\alpha\gamma})$ and $(C_1^{\gamma\alpha}, C_2^{\gamma\alpha})$ respectively, are constant. There exists a class of exact solutions to equation 31 which are often referred to as being shape-preserving [65]. In Coates' paper, those solutions were used. It is assumed that the local equilibrium is maintained at the α/γ interface. Hence $(C_1^{\alpha\gamma}, C_2^{\alpha\gamma})$ and $(C_1^{\gamma\alpha}, C_2^{\gamma\alpha})$ are located on the points at $\alpha/\alpha+\gamma$ and $\alpha+\gamma/\gamma$ phase boundaries, respectively, of the T_0 isotherm and these points are joined by a tie-line. With the solutions of equation 31, the only remaining problem is the mass conservation conditions which apply at the α/γ interface. These boundary conditions are of the general form:

$$\begin{aligned} \mathbf{n}\cdot\mathbf{V}(C_i^{\alpha\gamma} - C_i^{\gamma\alpha}) &= \mathbf{n}\cdot\mathbf{J}_i|_{\text{interface}} \\ &= \mathbf{n}\cdot\nabla C_i|_{\text{interface}} \end{aligned} \tag{32}$$

where $\mathbf{n}$ is a unit vector normal to the interface and $\mathbf{V}$ is the velocity of the interface. Ham was shown that for shape-preserving growth of precipitate particles of uniform interface concentrations, when the appropriate solutions of Eq. 31 are applied to Eq. 32, one obtains:

$$\frac{1}{2}(C_i^{\alpha\gamma} - C_i^{\gamma\alpha})\xi F(\xi, D_i) = -D_i(\bar{C}_i - C_i^{\gamma\alpha})F'(\xi, D_i) \quad (i = 1, 2) \tag{33}$$

where the constant ξ is a measure of the precipitate growth rate, $F(\xi, D_i)$ arises out of the solution to Eq. 31 and its functional form depends on the shape of precipitate particle. Here, the fractional compositions are defined:

$$f_i \equiv \frac{\bar{C}_i - C_i^{\gamma\alpha}}{C_i^{\alpha\gamma} - C_i^{\gamma\alpha}} = \frac{\bar{C}_i - C_i^{\gamma\alpha}}{(C_i^{\alpha\gamma} - \bar{C}_i) + (\bar{C}_i - C_i^{\gamma\alpha})} \tag{34}$$

It is obvious that the fractional component f_i of component i goes from 0 at negligible supersaturation, $(\bar{C}_i - C_i^{\gamma\alpha}) = 0$ to 1 at the maximum supersaturation $(C_i^{\alpha\gamma} - \bar{C}_i) = 0$. Combining equation 33 and 34 results to:

$$f_i = -\frac{\xi F(\xi, D_i)}{2D_i F'(\xi, D_i)} \tag{35}$$

For planar growth, the velocity of the precipitate-matrix interface i simply:

$$V = \frac{1}{2}\xi t^{-1/2} \tag{36}$$

And it is convenient to define:

$$\xi = \eta_1\sqrt{D_1} = \eta_2\sqrt{D_2} \tag{37}$$

where η_1 and η_2 are constants. Hence, the D_i and ξ appear only as the ratio $\xi/\sqrt{D_i}$ in the equation 35 which allows to describe f_i as a function of

η_i. In short,

$$f_i = f_i(\eta_i) \tag{38}$$

The values (f_1, f_2) mean that the fractional position in the square that made of four lines:

1. $C_1 = C_1^{\alpha\gamma}$ and $C_1 = C_1^{\gamma\alpha}$
2. $C_2 = C_2^{\alpha\gamma}$ and $C_1 = C_2^{\gamma\alpha}$

For certain ratio of D_1 to D_2, it decide also the ratio between η_1 and η_2 from equation 37 and it is possible to find number of (f_1, f_2) which satisfy those ratios. Important fact is that the those values, (f_1, f_2), will have the acting tie-line which connects $(C_1^{\alpha\gamma}, C_2^{\alpha\gamma})$ and $(C_1^{\gamma\alpha}, C_2^{\gamma\alpha})$ for given ratio of D_1 to D_2. If component 1 is X and component 2 is C, then it is the case when $D_2/D_1 = \infty$. Moreover, it is equivalent that $f_1 = 1$ with NPLE and $f_2 = 0$ with PLE for the $D_2/D_1 = \infty$.

2.6.2 Pearlite transformation in ternary system

It is important to consider the co-operative growth nature of pearlite when it is analysed in the content of thermodynamics. Because substitutional element X is alloyed, the partitioning behaviour of X becomes important to account. Carbide forming elements such as Mn, Cr, and Mo would partition to the pearlitic cementite whereas Si, Ni, and Co would tend to segregate to the ferrite. Most of partitioning studies used analytical electron microscopy and the results are expressed as partitioning coefficient K_{X} which is defined as the ratio of concentration of alloying element in cementite to that in ferrite:

$$K_{\mathrm{X}} = \frac{(C_{\mathrm{X}}/C_{\mathrm{Fe}})_\theta}{(C_{\mathrm{X}}/C_{\mathrm{Fe}})_\alpha} \tag{39}$$

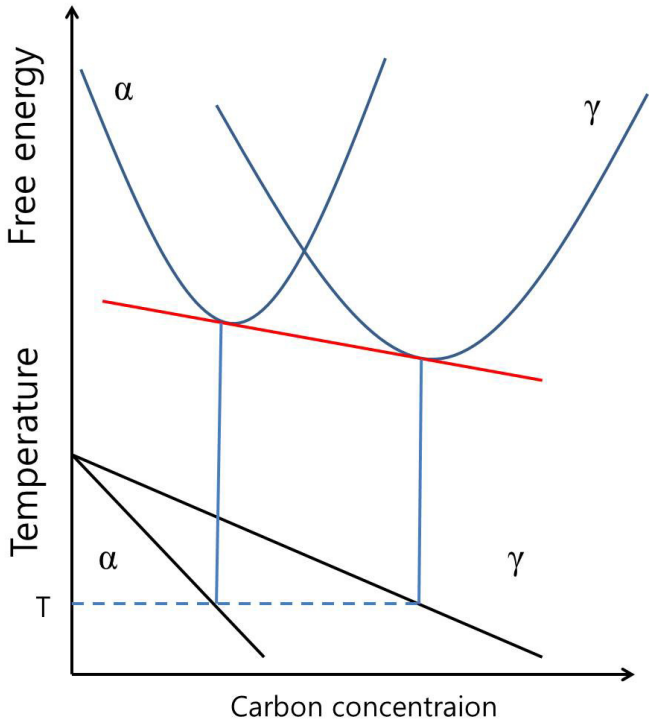

Figure 10: The relationship between phase diagram and free energy curves.

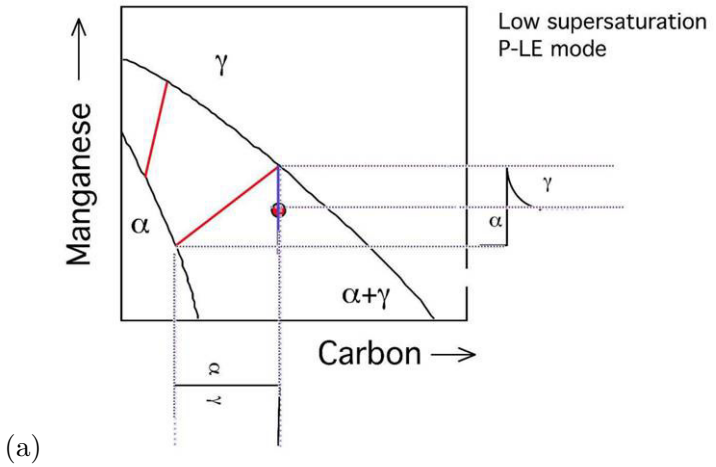

(a)

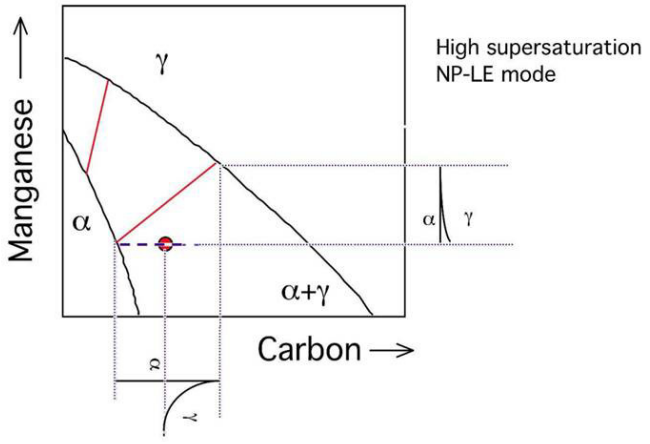

(b)

Figure 11: Schematic ternary steel phase diagram in the corner of α and γ related phase field: (a) PLE mode of proeutectoid ferrite growth and (b) NPLE mode of proeutectoid ferrite growth in the parent austenite.

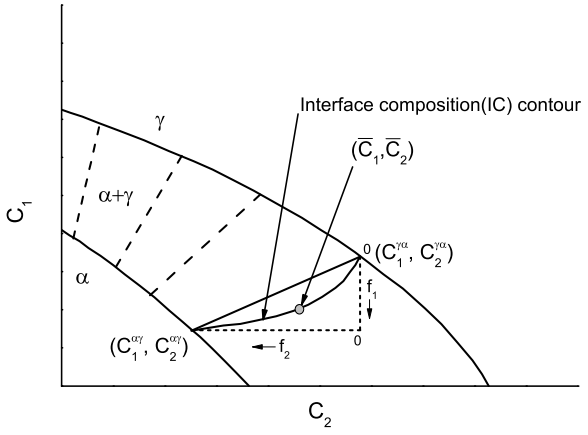

(a)

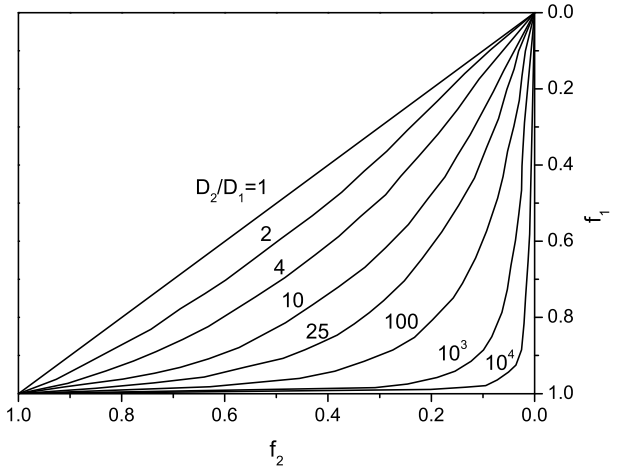

(b)

Figure 12: (a) Explanation for interface composition (IC) contours which is group of compositions having same acting tie-line at certain temperature and diffusivity ration. (b) The change of IC contours by the diffusion coefficient rate between alloying element '1' and '2' noted as fractional position.

where, C_{X} and C_{Fe} are the weight fraction of X and Fe respectively. Most of these alloying additions retard the growth rate of pearlite through their effect on the carbon concentration gradient.

Picklesimer *et al.* [66] measured the growth rate of pearlite based on the modified absolute rate theory of the form:

$$v = b\Delta T \Delta G \exp\left(\frac{-Q}{RT}\right) \tag{40}$$

where v is the growth rate in $\mathrm{mm\,s^{-1}}$, b is a constant, ΔG is the free energy difference of austenite to pearlite transformation and Q is the activation energy. They argued that the rate of pearlite growth is neither controlled by Mn diffusion and probably not by carbon. In their theory, decrease of pearlite growth rate by alloying X is due to increase of activation energy for those atomic movements at the moving boundary which are required because of the differences in crystal structure of austenite and ferrite and cementite in contact with it. They observed the partitioning behaviour of Mn stop below 640 °C where the chemical analysis was done from extracted carbide replicas. However, it was measured after 24 h at transformation temperature and the carbides came from far behind of transformation front.

Razik *et al.* [67] reported that the electron probe micro-analyser was not an effective tool for partitioning studies owing to its resolution (2 μm) as comparing with the thickness of cementite lamellae is far less than 2 μm. They used the analytical electron microscopy to measure the composition of manganese in pearlitic cementite and ferrite. The study was done with 1.08 and 1.8Mn wt% eutectoid steels. They observed the partitioning coefficient of manganese between pearlitic cementite and ferrite becomes unity.

The partitioning of Mn decreased from eutectoid temperature and it ceased below 683 °C and 649 °C for 1.08 and 1.8Mn wt% respectively. However, they used the interface compositions in the Fe-C binary phase diagram. Because the effect of Mn changes the phase diagram very differently compared to binary system, this is clearly not appropriate procedure to find acting tie-line. In other work of Razik et al [57] *et al.*, they studied Fe-1.29Cr-0.8C wt% and observed partitioning even lower than the reported no-partitioning temperature as 703 °C. Both of studies assumed either volume and boundary diffusion, but those mechanisms cannot properly explain experimentally measured growth rate.

Finding the acting tie-line at the interface of pearlite/austenite was studied by Hillert [38]. He tried to categorise the pearlite transformation using phase diagram. It was an excellent attempt to explain thermodynamical background of pearlite transformation using PLE and NPLE model. In his report, the divergent pearlite was the result of driving force decreasing due to the pearlite composition. Divergent pearlite forms only in $\alpha + \gamma + \theta$ three phase field, and the pearlite always have higher alloying element concentration than parent austenite that is the reason why the free energy for diffusion is ceased when the composition of the system reached the γ corner of three phase field. His theory was supported by the measurement of Hutchinson *et al.* [21]. Hutchinson and his colleagues measure the composition profile of Mn across the pearlite/austenite interface over the transformation time and temperature for various Fe-C-Mn system using analytical transmission microscopy. Hillert used PLE and NPLE for the pearlite transformation in $\alpha + \theta$ phase field. He only analysed the area which both of ferrite and cementite grow with PLE or NPLE and, for those areas, it was also well explain Hutchinson's data. However, those PLE and

NPLE assumptions cannot explain all area of $\alpha+\theta$ phase field. Pandit and Bhadeshia [11] used both of volume and boundary diffusion mechanism for pearlite growth and used PLE assumptions at the pearlite/austenite interface. However, it cannot give solutions that compromise both mass balance and local equilibrium condition. Pandit and Bhadeshia use the straight tie-line which is passing through the mean composition of the system rather than use PLE or NPLE condition. However, their solution is clearly incorrect because that lose both mass balance and thermodynamical nature.

2.7 Deriving Mixed-Diffusion Growth Rate Equation

The mixed-diffusion of pearlite growth rate equation was suggested by Pandit and Bhadeshia[10]. Mixed-diffusion equation is well explained in the case of the iron-carbon binary system without any artificial factor relating volume and boundary fluxes.

$$v = \left(2D_V + \frac{12D_B\delta}{S}\right)\frac{S}{S_\alpha S_\theta}\left(\frac{c_e^{\gamma\alpha} - c_e^{\gamma\theta}}{c^{\theta\gamma} - c^{\alpha\gamma}}\right)\left(1 - \frac{S_C}{S}\right) \tag{41}$$

Eq. 41 is derived from a flux balance between pearlite and austenite. v is the growth rate of pearlite, D_V and D_B are volume and boundary diffusion coefficients in austenite respectively, S is the interlamellar spacing, S_C is the critical interlamellar spacing when interface energy between ferrite and cementite consumes total free energy in the system (so pearlite never grow), and c^{ab} are composition on phase 'a' have interface with phase 'b'. Phases are ferrite (α), cementite (θ), and austenite (γ).

The flux in the austenite, from the front of ferrite to the front of cementite is,

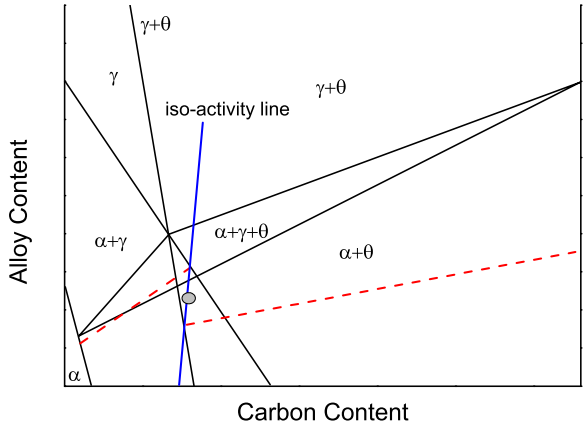

(a)

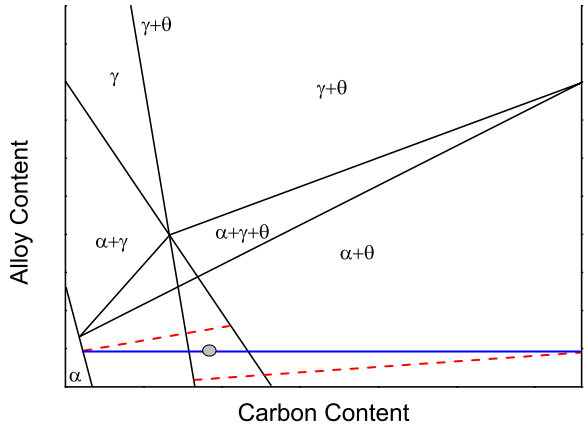

(b)

Figure 13: Pearlite growth on the phase diagram when the pearlite grows as (a) PLE mode, (b) NPLE mode

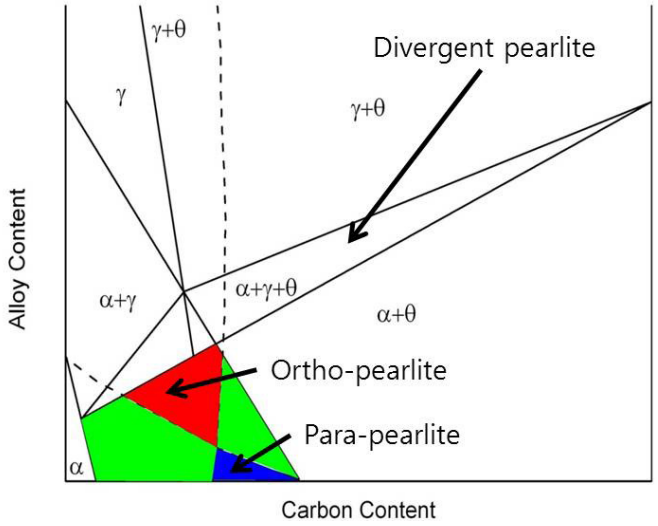

Figure 14: The regions which are distinguished by growth mode of pearlite. When the cementite and ferrite grow with PLE mode (in red area), that pearlite called ortho-pearlite. When the both θ and α is in NPLE region, it called para-pearlite growth [38]. However there are no analyses on green area.

$$J_V = \frac{D_V b S_\alpha}{V_\mathrm{m}} \frac{c^{\gamma\alpha} - c^{\gamma\theta}}{S_\alpha/2}$$
$$J_B = \frac{12 D_B b \delta}{V_\mathrm{m}} \frac{c^{\gamma\alpha} - c^{\gamma\theta}}{S} \tag{42}$$

where b is the arbitrary length which is normal to growth direction, δ is a length of boundary, V_m is the molar volume and is considered as same for all the phases involved. This diffusion causes the edgewise growth of α lamellae in γ with a velocity v and can be written as equation 17:

$$J = \frac{v b S_\alpha}{V_\mathrm{m}}(\bar{c} - c^{\alpha\gamma}) = \frac{v b S^\theta}{V_m}(c^{\theta\gamma} - \bar{c}) = \frac{v b S_\alpha S_\theta}{S V_\mathrm{m}}(c^{\theta\gamma} - c^{\alpha\gamma})$$

Combining Eq. 42 and 17 will result in Eq. 41.

3 Mixed Diffusion Controlled Growth of Pearlite in Fe-C Binary System

3.1 Boundary diffusion coefficient of carbon

Because there is a lack of boundary diffusion data for carbon, the coefficient needs to be deduced from other data. In this thesis, the measured pearlite growth rate in Fe-C binary system was used to extract the boundary diffusion coefficient. This kind of an attempt with mixed diffusion controlled model is not the first. Hashiguchi and Kirkaldy [9] did the first extraction of boundary diffusion coefficient of carbon from the pearlite growth data based on mixed diffusion model. However, their carbon diffusivity in pearlite/austenite boundary was not able to explain the higher diffusion activation energy for interface than lattice. Their mixed diffusion equation accounted for many effects that included unimportant factors. Thus, the activation energy for boundary diffusion of carbon was over-fitted and showed larger value than that for volume diffusion. Pandit and Bhadeshia [10] constructed the mixed diffusion equation of pearlite with only the edge-wise volume diffusion and side-wise boundary diffusion. In their equation, the effects except diffusion, such as capillarity and surface tension, were not taken account during the modelling. The procedure of extracting carbon boundary diffusivity in the paper of Ashwin and Bhadeshia underestimate the difference between experimental methods used to measure pearlite growth rate. There are three known methods to observe the pearlite growth rate.

One is the maximum nodule radius method (MNR method)[68]. MNR is the method that measure the radius of the largest colony in the microstructure and the transformation time, then calculate pearlite growth rate with

them. Therefore, MNR method always give the maximum growth rate of the pearlite during the transformation. It is important that the radius of colony should be observed before the impingement happens and the incubation time which is the period before the actual growth start have not to be considered. MNR is hardly measure the growth rate with non-hemispherical colony shape, time dependency, and impingement. Cahn and Hagel method (CH method) was developed for measuring time-dependent pearlite growth rate [69]. This evaluates the average growth rate of the observed pearlite colonies as:

$$\bar{v} = \frac{1}{A_f}\frac{\mathrm{d}r}{\mathrm{d}t} \tag{43}$$

where, $\bar{v}$ is the average growth rate, A_f is the instantaneous pearlite surface area per unit volume available for migration, r is the averaged radii of colonies, and t is the time for transformation. The value of A_f and r can be measured using standard point counting method [70]. The last one is particle size analysis method (PSA method). PSA method approximate the pearlite nodule as a sphere, then compute a size distribution of 'circle' diameters observed on a optical micrograph of a plane that is polished and etched. The distribution curves of circle diameters per unit volume have informations of both growth and nucleation. The Johnson-Mehl equation [71] used for determining the nucleation rate at early stage of transformation and growth rate. Also, in-situ neutron depolarisation [72] and three-dimensional X-ray microscopy [73] can be used to measure individual colony.

Among the above methods, latter two, CH and PSA methods, take the average of observed pearlite nodules. However, the models, or the growth rate equations, predict the maximum velocity of the transformation

front. Therefore, it is reasonable that the boundary diffusion coefficient of carbon is deduced from using the MNR method result. In this chapter, the boundary diffusivity of carbon will extracted from the experimental results from Frye et al. [74] which measured the pearlite growth rate with MNR method.

3.2 Methods

The diffusion-controlled growth of pearlite in a binary steel, including both the volume and boundary fluxes, is given by Pandit and Bhadeshia [10] (Eq. 41):

$$v = \left(2D_V + \frac{12sD_B\delta}{S}\right)\frac{S}{S_\alpha S_\theta}\left(\frac{c_e^{\gamma\alpha} - c_e^{\gamma\theta}}{c^{\theta\gamma} - c^{\alpha\gamma}}\right)\left(1 - \frac{S_C}{S}\right)$$

where v is the growth rate, s is the arbitrary length which is normal to growth direction, D_V and D_B are volume and boundary diffusion coefficients in austenite respectively, S is the interlamellar spacing, S_C is the critical interlamellar spacing when the α/θ interfaces that are created during pearlite growth consume all the available free energy so that the growth rate becomes zero. $c^{\gamma\theta}$ is the concentration in austenite that is in equilibrium with cementite, and other terms like this have similar meaning. These equilibrium compositions are here calculated using ThermoCalc with the TCFE6 database [41].

In equation 41, the values of interlamellar spacing S, the diffusion coefficients and boundary thickness $\delta = 2.5\,\text{Å}$ can be obtained from the published literature [74, 5, 61, 67]. The diffusivity of carbon in austenite is

Table 1: Calculated interface C concentrations (at.%).

	$c_{\mathrm{C}}^{\gamma\theta}$	$c_{\mathrm{C}}^{\theta\gamma}$	$c_{\mathrm{C}}^{\gamma\alpha}$	$c_{\mathrm{C}}^{\alpha\gamma}$
866 K	2.10	0.25	8.33	0.127
892 K	2.35	0.25	7.33	0.124
913 K	2.54	0.25	6.53	0.120
933 K	2.75	0.25	5.78	0.115
963 K	3.05	0.25	4.68	0.104
978 K	3.21	0.25	4.16	0.098
981 K	3.24	0.25	4.06	0.097

concentration dependent, so a weighted average value is used instead [45]

$$\overline{D}_V = \int_{c^{\gamma\theta}}^{c^{\gamma\alpha}} \frac{D\{\overline{c}, T\}}{c^{\gamma\alpha} - c^{\gamma\theta}} \, \mathrm{d}c^{\gamma} \tag{44}$$

where $\overline{c}$ is the mean carbon concentration in the steel.

3.3 Results

There are three methods that were shown above for measuring the growth rate of pearlite: particle size analysis method [61], the maximum nodule radius method [68] and Cahn & the Hagel method [69]. The experimental data of Frye *et al.* [74] based on the maximum nodule radius method were used to obtain the boundary diffusion coefficient of carbon. This is because the method is based on the assumption that the largest module correctly represents the actual growth rate, whereas the other two methods rely on averaged values. The term $\frac{S_{\mathrm{C}}}{S}$ was calculated by taking derivative of equation 41 with respect to the interlamellar spacing, S, and solving the

resulting equation for S_C that satisfies:

$$\frac{\mathrm{d}v}{\mathrm{d}S} = 0 \tag{45}$$

Equations 41 and 45, when used with the experimental value of v, have two unknowns. They can therefore be solved iteratively to find the values of D_B and $\frac{S_C}{S}$. As a result, the boundary diffusion coefficient for carbon is found to be

$$D_B^C = 1.84 \times 10^{-3} \exp\left(-\frac{124995\,\mathrm{J\,mol^{-1}}}{RT}\right) \qquad \mathrm{m^2\,s^{-1}} \tag{46}$$

where R is the gas constant and T is the temperature, in Fig. 15. The boundary diffusion activation energy, $Q_B = 125\,\mathrm{kJ\,mol^{-1}}$, is lower, as it should be, than the corresponding value for diffusion in the volume of the austenite, $Q_V = 135\,\mathrm{kJ}$.

Fig. 16 shows calculations based on equation 41 and the experimental data of Brown and Frye *et al.* The carbon diffusion coefficient derived using Frye's data has been applied unmodified to the data from Brown and Ridley, and yet there is excellent closure between experiment and theory. Fig. 17 illustrates the ratio of volume to boundary diffusion fluxes and the deependence of S on the transformation temperature. As expected, the boundary flux dominates at low temperatures where diffusion within the austenite lattice is relatively sluggish. Fig. 17b is the set of all solutions which satisfying equation 45. When D_V is negligible relative to D_B, $\frac{S_C}{S}$ tends towards $\frac{2}{3}$ in the low temperature range.

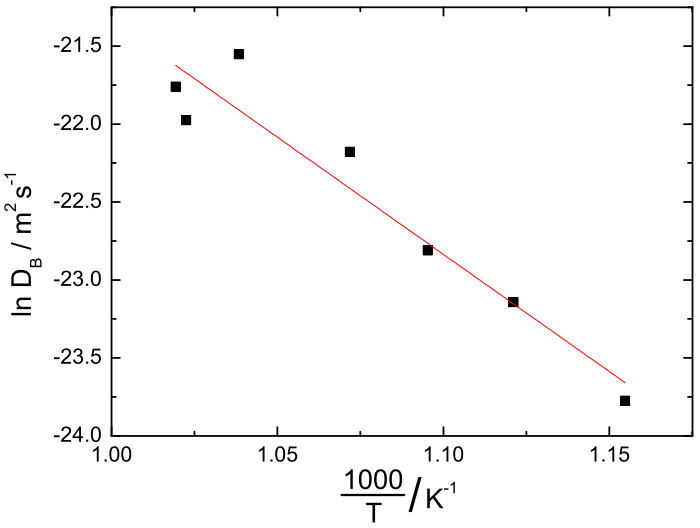

Figure 15: Arrhenius plot from which D_B was derived based on experimental data on Fe-0.8 wt%C steel assuming mixed diffusion-controlled pearlite growth.

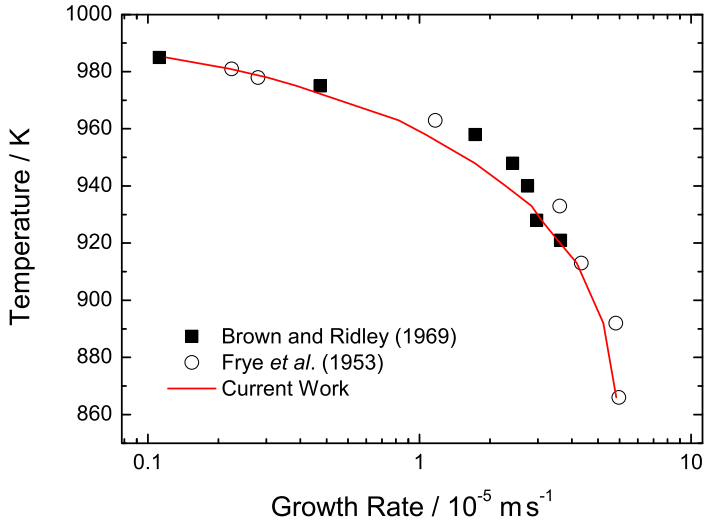

Figure 16: Calculated growth rate of pearlite for mixed diffusion model compared against experimental data.

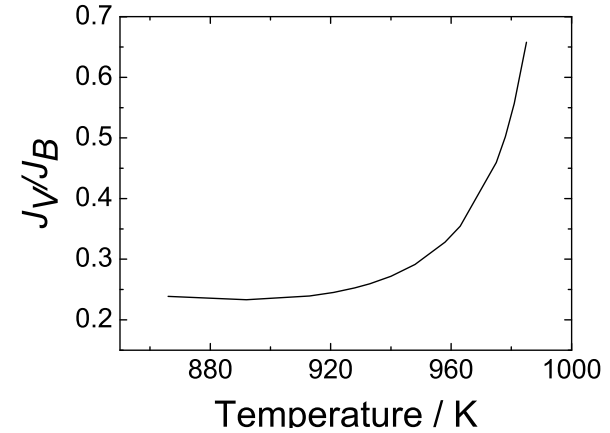

(a)

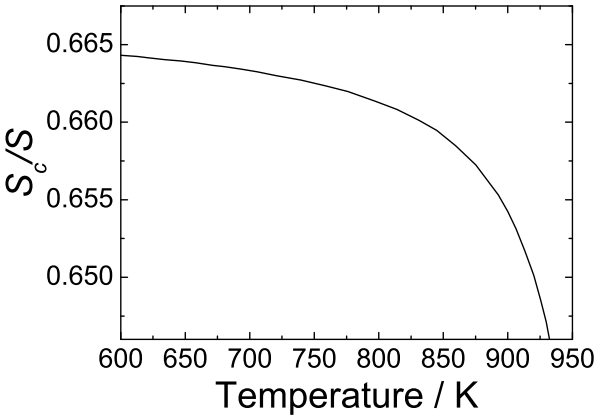

(b)

Figure 17: (a) The ratio of volume to boundary flux versus temperature in Fe-C eutectoid steel. (b) The ratio of critical interlamellar spacing, S_C to S as a function of temperature.

3.4 Interface energy

The interface energy between ferrite and cementite per unit area, $\sigma^{\alpha\theta}$, has critical role during the pearlite transformation. It is not directly included in the growth rate equation but the critical interlamellar spacing, S_C have $\sigma^{\alpha\theta}$ as variable. This is because the $\sigma^{\alpha\theta}$ always consumes the total free energy as the pearlite colony grows. Zener [2] has shown that the pearlite growth rate have maximum value when the interface energy between ferrite and cementite is half of total free energy available for transformation assuming volume diffusion controlled growth. Kramer *et al.* calculated the $\sigma^{\alpha\theta}$ using Zener's free energy and spacing data to be $0.7\,\mathrm{J\,m^{-2}}$ [75]. They calculated the interface energy, $\sigma^{\alpha\theta}$, using a calorimetric method.

Das *et al.* [76] and, Deb and Chaturvedi [77] measured the energy of ferrite/cementite interface for coarsening of cementite particles in ferrite matrix steel (Fig. label interface). The interface energy was obtained from the coarsening rate constant, which was determined by fitting experimental growth rate data. It is worth noting that these data for a different morphology (spherical) of ferrite/cementite interface shows lesser energy value than for a lamellar pearlite. Martin and Sellers calculated the interface energy for lenticular cementite precipitates on a ferrite grain boundaries from dihedral angle measurements and reported a value of $0.52 \pm 0.13\,\mathrm{J\,m^{-2}}$. Embedded atom method with first-principles method was used to compute the interface energy between ferrite and cementite in Fe-C system by Ruda *et al.* [78]. They reported the value of $0.615\,\mathrm{J\,m^{-2}}$. There was no mention about the temperature at which this calculation was done, but it can be assumed to be same at $0\,\mathrm{K}$ as usually used by first-principles calculations.

In other point of view, it is possible that govern the interface energy of ferrite/cementite interface from the pearlite growth rate because the term S_{C}. In this thesis, the interface energy between ferrite and cementite, $\sigma^{\alpha\theta}$, was deduced from the results of fig. 17 and following equation [9]:

$$\sigma^{\alpha\theta} = \frac{1}{2} S_{\mathrm{C}} \Delta G \tag{47}$$

where the ΔG is a total free energy of the system for transformation. The free energy is calculated using Thermo-Calc[41], TCFE6 database. The interface energy values calculated in current thesis are illustrated in fig. label interface. Comparing the interface energies calculated from pearlite growth rate measurements and the independently measured values, the discrepancies between them are large for the lower transformation temperatures, relative to the data based on coarsening reactions and dihedral angle measurements. Both of the measurements are done at which the transformation is kinetically slow, therefore, it is possible that the measured values are affected by the segregation of solutes to the interface, which might lead to a reduction in energy.

3.5 Conclusions

The mixed diffusion-controlled growth of pearlite is revised with considering the relationship between experimental data and maximum growth rate spacing criteria. The spacing criteria is also mathematically solved to analysis the temperature-S_{C} relationship. The critical interlamellar spacing S_{C} indirectly shows the ratio change between volume and boundary flux, for example, S_{C} converges to $\frac{2}{3}$ as temperature goes down and this can be well explained by low activation energy of boundary diffusivity. Because of lacking boundary diffusion data, the boundary diffusion coefficient of carbon

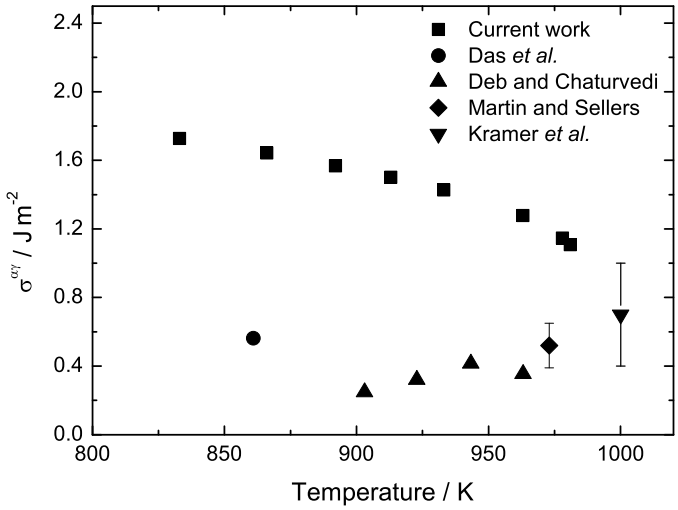

Figure 18: Comparison of calculated ferrite/cementite interface energy per unit area based on Thermo-Calc (TCFE6 database) to independently measurements.

is deduced from the experimental data of Frye *et al.* [74]. The expected pearlite growth rate in Fe-C system shows an excellent agreement with the experimental data of Brown and Ridley [61] which is not used for deducing boundary diffusion coefficient of carbon.
The interface energy is calculated using maximum growth rate spacing criteria, and compared to reported independent measurements. The energy is higher than reported values at all temperature range, possibly because the reported values are measured at slow coarsening of cementite and the effect of segregation might reduced the value.

4 Mixed Diffusion Controlled Growth of Pearlite in Fe-X-C (X=Mn, Cr, Co, Ni) Ternary System

4.1 Methods

In Fe-C binary steels, the interface composition at ferrite/austenite and cementite/austenite boundary is easily found by simple thermodynamic calculation. This is because the tie line between α/γ and θ/γ in Fe-C phase diagram is unique during isothermal transformation.

To maintain local equilibrium condition, the situation is more complex in Fe-C-X steels containing a substitutional solute (X) in addition to interstitial carbon. Local equilibrium requires the compositions at the interface to be maintained at levels that are consistent with a tie-line of the Fe-C-X phase diagram. At a constant temperature, this is in general not possible to achieve for the tie line passing through $\overline{c}_{\mathrm{Mn}}, \overline{c}_{\mathrm{C}}$ because the rate at which each solute is partitioned must then equal to that at which it is carried away from the interface by diffusion. It is necessary therefore that

$$\text{at } \alpha/\gamma \text{ interface: } \begin{cases} v(c_{\mathrm{C}}^{\gamma\alpha} - c_{\mathrm{C}}^{\alpha\gamma}) = -D_{\mathrm{C}}\nabla c_{\mathrm{C}} \\ v(c_{\mathrm{X}}^{\gamma\alpha} - c_{\mathrm{X}}^{\alpha\gamma}) = -D_{\mathrm{X}}\nabla c_{\mathrm{X}} \end{cases} \tag{48}$$

$$\text{at } \theta/\gamma \text{ interface: } \begin{cases} v(c_{\mathrm{C}}^{\gamma\theta} - c_{\mathrm{C}}^{\theta\gamma}) = -D_{\mathrm{C}}\nabla c_{\mathrm{C}} \\ v(c_{\mathrm{X}}^{\gamma\theta} - c_{\mathrm{X}}^{\theta\gamma}) = -D_{\mathrm{X}}\nabla c_{\mathrm{X}} \end{cases} \tag{49}$$

where the subscripts identify the solute. Given that $D_{\mathrm{X}} \ll D_{\mathrm{C}}$, it becomes impossible to simultaneously satisfy either equation 48 or 49 if the tie-line passing through $\overline{c}_{\mathrm{X}}, \overline{c}_{\mathrm{c}}$ is selected.

Pandit and Bhadeshia [11] argued that in the context of experimental data, local equilibrium could not be assumed for both the α/γ and θ/γ interfaces. They therefore proceeded to adopt the tie line connecting the

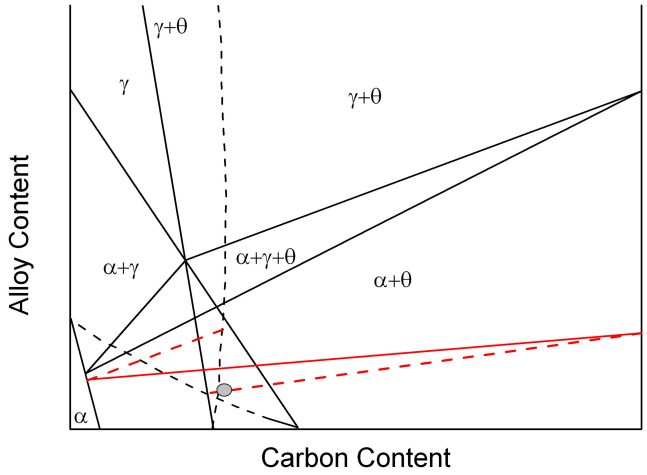

Figure 19: Fe-Mn-C phase diagram and tie-lines (red) used in [11].

θ/γ interface passes through $\overline{c}_{\mathrm{X}}, \overline{c}_{\mathrm{c}}$ (Fig. 19), neglected the role of carbon and calculated the growth rate on the basis of the diffusion of manganese through the interfaces rather than the volume ahead of the interface.

All of above work only considered the case of $D_{\mathrm{X}} \ll D_{\mathrm{C}}$ even some of them dealing with boundary diffusion. The natural question arises when the boundary diffusion has an important role as a diffusion short circuit; Does $D_{\mathrm{X}} \ll D_{\mathrm{C}}$ still stand for the boundary diffusion and mixed diffusion controlled transformation?

Coates [62] already studied the case when the ratio D_{X} to D_{C} is finite for the single phase transformation. He used the solution of diffusion equation which is reported by Ham [65]. Pearlite is cooperative growth of ferrite and cementite so it needs other solution. Hashiguchi and Kirkaldy

[9] solved the diffusion equation of pearlite with considering boundary diffusion of carbon. However, that solution deduced physically unlike activation energy of carbon boundary diffusivity. In previous chapter, simplified solution of pearlite diffusion equation with mixed diffusion controlled growth well describes the experimental data and physically reasonable boundary diffusion coefficient of carbon. Thus, that solution is used to find interface composition when the ratio D_{X} to D_{C} is finite.

A different procedure avoiding the difficulties encountered in ref. [11], can be based on the following equations that are analogous with equation 41:

$$\begin{aligned} v_{\mathrm{C}} &= \left(2D_V^{\mathrm{C}} + \frac{12sD_B^{\mathrm{C}}\delta}{S}\right)\frac{S}{S_\alpha S_\theta}\left(\frac{c_{\mathrm{C}}^{\gamma\alpha} - c_{\mathrm{C}}^{\gamma\theta}}{c_{\mathrm{C}}^{\theta\gamma} - c_{\mathrm{C}}^{\alpha\gamma}}\right)\left(1 - \frac{S_C}{S}\right) \\ v_{\mathrm{X}} &= \left(2D_V^{\mathrm{X}} + \frac{12sD_B^{\mathrm{X}}\delta}{S}\right)\frac{S}{S_\alpha S_\theta}\left(\frac{c_{\mathrm{X}}^{\gamma\alpha} - c_{\mathrm{X}}^{\gamma\theta}}{c_{\mathrm{X}}^{\theta\gamma} - c_{\mathrm{X}}^{\alpha\gamma}}\right)\left(1 - \frac{S_C}{S}\right) \end{aligned} \tag{50}$$

where the velocities v_{C} and v_{X} are calculated on the basis of the diffusion of only carbon or only manganese, respectively. Clearly, since there is only one transformation front, the equations must be solved such that $v_{\mathrm{C}} = v_{\mathrm{X}}$. Bearing in mind that the interlamellar spacing is also identical in these equations, a further condition arises that:

$$\frac{D_{eff}^{\mathrm{C}}}{D_{eff}^{\mathrm{X}}} = \frac{R_{\mathrm{X}}}{R_{\mathrm{C}}} \qquad \text{with} \qquad \begin{cases} D_{eff}^i \equiv D_V^i + \frac{6sD_B^i\delta}{S} \\ R_i \equiv \frac{c_i^{\gamma\alpha} - c_i^{\gamma\theta}}{c_i^{\theta\gamma} - c_i^{\alpha\gamma}} \end{cases} \tag{51}$$

The D_{eff}^i is effective diffusion coefficient for mixed diffusion-controlled growth and R_i condition ensures that the weighted average of the ferrite

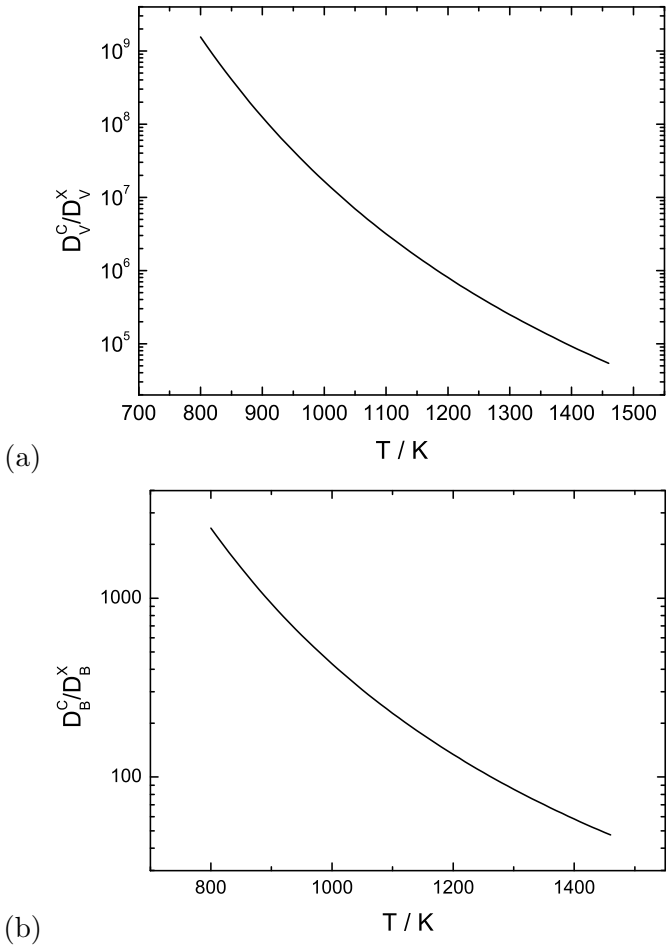

Figure 20: The diffusivity ratio of carbon to substitutional solute X for (a) volume diffusion and (b) boundary diffusion

and cementite yields the mean composition of the steel. With these two constraints and in addition the local equilibrium condition, it has been found possible to find unique interface compositions at the growth front by coupling the conditions and the velocity equations to thermodynamic calculations using Thermo-Calc with TCFE6 database; the application package was designed as follows:

- a trial θ/γ interface composition is set, selected from possible such tie-lines for the given transformation temperature.
- The α/γ interface composition tie-line is selected such that $\overline{c^{\alpha\gamma}_{\mathrm{C,X}},\ c^{\theta\gamma}_{\mathrm{C,X}}} \ni \bar{c}_{\mathrm{C,X}}$ (where $\overline{c^{\alpha\gamma}_{\mathrm{C,X}},\ c^{\theta\gamma}_{\mathrm{C,X}}}$ means the line connecting the compositions of ferrite and cementite, and $\bar{c}_{\mathrm{C,X}}$ is average composition in the system).
- If equation 51 is not satisfied by these choices then the process is repeated until a solution is found.
- This solution provides the interface compositions to substitute into equation 50 to calculate the single velocity $v = v_{\mathrm{C}} = v_{\mathrm{X}}$ of the transformation interface.

4.2 Results and Discussion

4.3 Mixed diffusion-controlled growth for Fe-X-C

The diffusion coefficients of substitutional solute in the boundary and austenite are from Fridberg *et al.* [54]:

$$D_B^X = 2.16 \times 10^{-4} \exp\left(-\frac{155000\,\mathrm{J\,mol^{-1}}}{RT}\right) \qquad \mathrm{m^2\,s^{-1}} \qquad (52)$$

$$D_V^{\mathrm{Mn}} = 1.34 \times 10^{-4} \exp\left(-\frac{286000\,\mathrm{J\,mol^{-1}}}{RT}\right) \qquad \mathrm{m^2\,s^{-1}} \qquad (53)$$

There will be some uncertainty in D_B^X because it is assumed to be identical to that for the grain boundary diffusion of iron [54]. Equation 41 for the ternary system was tested against experimental data on 1 wt% Mn and 1.8 wt% Mn eutectoid steels from the work of Razik and Ridley [67].

As shown in Fig. 21, the mixed diffusion controlled-growth model explains the pearlite growth rates within an order of magnitude. A careful examination of the tie-lines operating during growth showed that at low temperatures, there is very little partitioning of manganese between the phases and partitioning becomes prominent for transformation at temperatures near the eutectoid. The extent of partitioning is predicted well using our mixed diffusion model, when compared against the microanalytical data of Hutchinson *et al.* [21] for Fe-3.50Mn-2.46C at.% steel at 898 K [21], Fig. 22. It is likely that during the 10 h treatment, soft impingement occurs and that might explain the discrepancy observed for that transformation time. The measured growth rate was $1.08 \times 10^{-8}\,\mathrm{m\,s^{-1}}$, which compares well with our calculated value of $9.46 \times 10^{-9}\,\mathrm{m\,s^{-1}}$.

Similar work is done for Cr, Ni, and Co. These atoms are selected by the neighbour of iron. This is because those atoms share the boundary diffusion coefficient which was reported by Fridberg *et al.* [54]. Therefore, they use eq. 52 for the boundary diffusion coefficient and volume diffusivity in below:

$$D_V^{\mathrm{Cr}} = 3.29 \times 10^{-4} \exp\left(-\frac{286000\,\mathrm{J\,mol^{-1}}}{RT}\right) \qquad \mathrm{m^2\,s^{-1}} \qquad (54)$$

Table 2: Calculated Mn concentrations (at.%); the mean value for the alloy is 1.07 at%.

	$c^{\gamma\theta}_{\mathrm{Mn}}$	$c^{\theta\gamma}_{\mathrm{Mn}}$	$c^{\gamma\alpha}_{\mathrm{Mn}}$	$c^{\alpha\gamma}_{\mathrm{Mn}}$
823 K	0.37	1.13	10.3	1.06
855 K	0.40	1.15	8.30	1.052
895 K	0.44	1.16	6.33	1.050
915 K	0.46	1.19	5.58	1.045
935 K	0.52	1.27	4.85	1.03
945 K	0.57	1.37	4.50	1.02
952 K	0.65	1.54	4.18	0.987
958 K	0.773	1.81	3.89	0.942

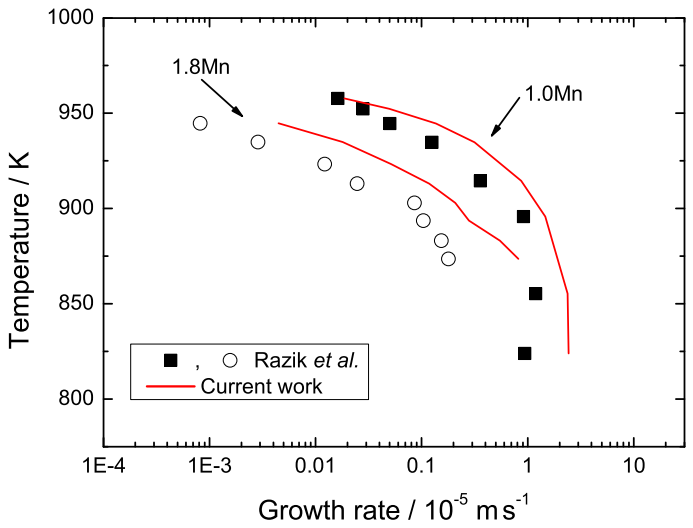

Figure 21: Mixed diffusion-controlled model applied to 1.0 and 1.8 wt%Mn eutectoid steels and experimental data for comparison.

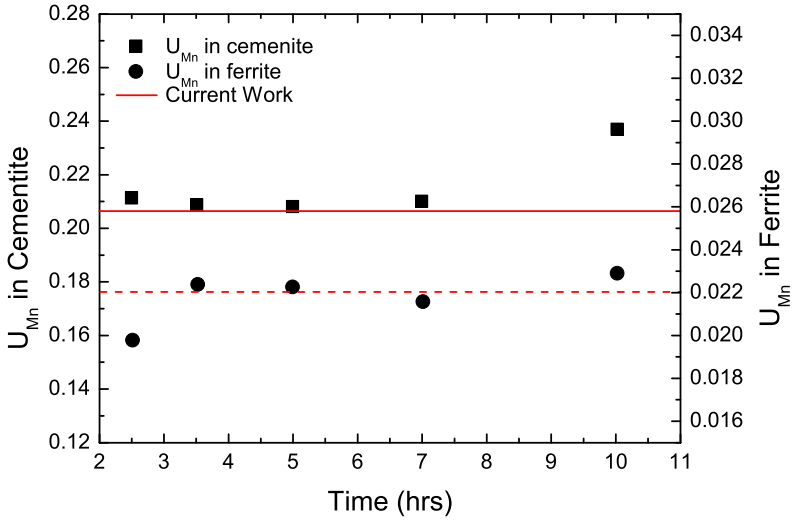

Figure 22: Mixed diffusion-controlled model predicts the interface composition of pearlite in Fe-3.50 at%Mn-2.46 at%C steel at 898 K. U_{Mn} is the ratio of the Mn to Fe atoms.

$$D_V^{\mathrm{Ni}} = 3.17 \times 10^{-5} \exp\left(-\frac{286000\,\mathrm{J\,mol^{-1}}}{RT}\right) \qquad \mathrm{m^2\,s^{-1}} \tag{55}$$

$$D_V^{\mathrm{Co}} = 3.31 \times 10^{-4} \exp\left(-\frac{286000\,\mathrm{J\,mol^{-1}}}{RT}\right) \qquad \mathrm{m^2\,s^{-1}} \tag{56}$$

When the mixed diffusion-controlled growth is applied to 2 and 3 wt% of Ni eutectoid steels and compared to experimental results of Brown and Ridley [61], it shows excellent agreement with the growth rate measured by MNR method as shown in Fig. 23. The experiment results are done at relatively higher temperature than the results Mn [67], thus discrepancies at low temperature is impossible to observe. The effect of Co to growth rate of pearlite was studied by Ridley and Burgess [79] and they measured the minimum interlamellar spacing. Those data are used for comparing with calculated pearlite growth rate based on mixed diffusion model in this thesis. Fig. 24 shows the comparing between calculated and measured pearlite growth rate. Similar as the results of Ni eutectoid steels, Co addition in eutectoid steels is well predicted by mixed diffusion-controlled growth.

When the mixed diffusion model is applied to Fe-Cr-C ternary system, the calculated results are about to be an order away from the experimental data of Chance and Ridley [20]. This is quite interesting compared to the results for Mn, Ni, Co. Large discrepancies appeared in Cr eutectoid steels can be explained with generalised Fick's first law:

$$\begin{pmatrix} J_{\mathrm{C}} \\ J_{\mathrm{X}} \end{pmatrix} = - \begin{pmatrix} D_{\mathrm{CC}} & D_{\mathrm{CX}} \\ D_{\mathrm{XC}} & D_{\mathrm{XX}} \end{pmatrix} \begin{pmatrix} \nabla c_{\mathrm{C}} \\ \nabla c_{\mathrm{X}} \end{pmatrix} \tag{57}$$

where J_i is the flux of component i, D_{ij} is diffusion coefficients of i affected by j, c_i is composition of i and, C and X are carbon and substitutional

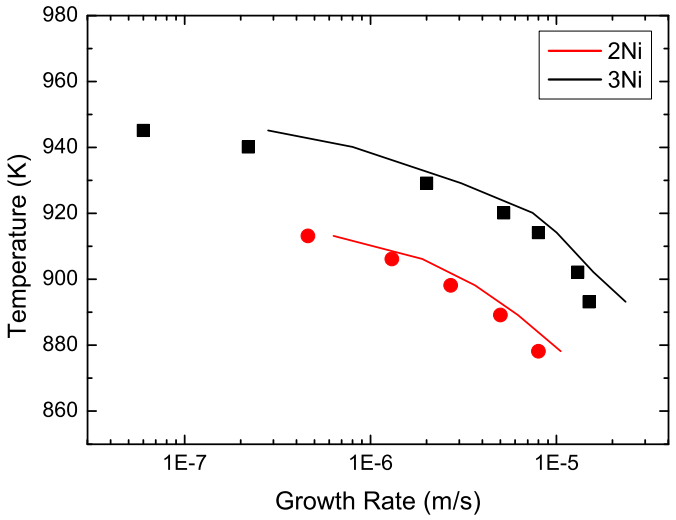

Figure 23: Mixed diffusion-controlled model applied to 1.98 and 3.00 wt%Ni eutectoid steels and experimental data for comparison. Points are experimental data from Brown and Ridley [61]. Lines are calculation work done in current thesis.

atom respectively. When the mixed diffusion-controlled model is derived, the off-diagonal term of diffusivity coefficient matrix in Eq. 57 are ignored. This off-diagonal diffusivities means that the chemical effect on each solute atoms. Ni and Co are known to have a low chemical interaction with carbon. On the other hand, Cr is a well-known strong carbide former, thus, the off-diagonal diffusivities may not be ignored.

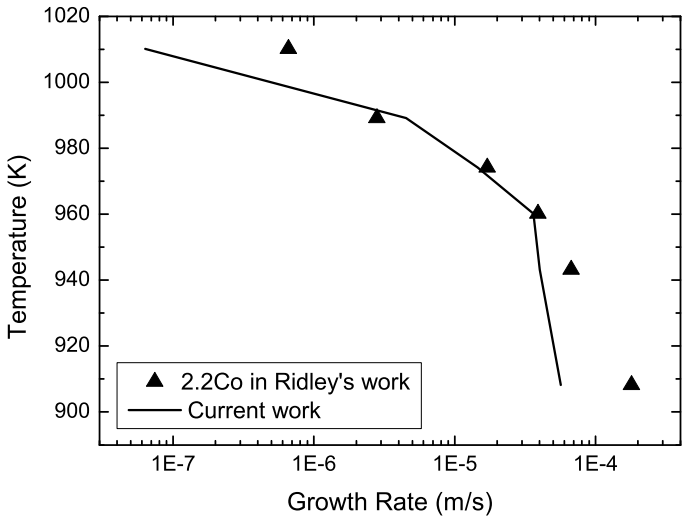

Figure 24: Mixed diffusion-controlled model applied to 2.2 wt%Co eutectoid steels and experimental data for comparison. The experimental data of Ridley and Burgess [79] (points) and calculated result in current work by mixed diffusion-controlled growth of pearlite (line).

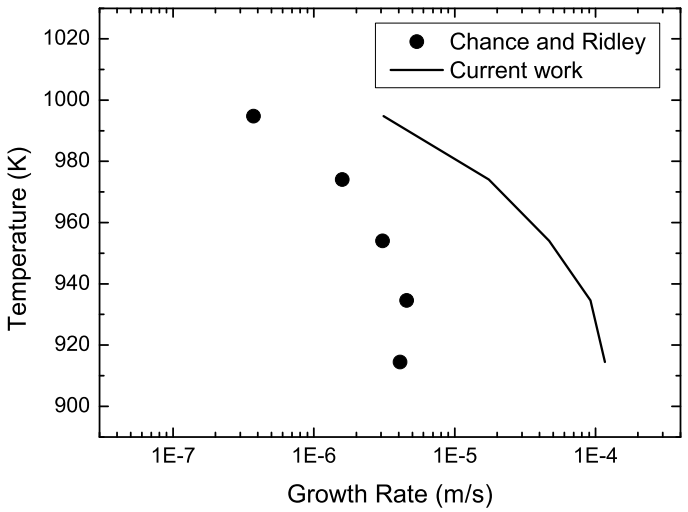

Figure 25: The experimental data is compared with mixed diffusion-controlled model in 1.4 wt%Cr eutectoid steels.

4.4 Metallography for the Fe-Mn-C system

In Fig. 21, it is seen that the measured growth rate at low temperatures tends to be significantly slower than that calculated. It was not felt that there are any options in modifying the theory to obtain a better fit; for example, if the transfer of iron atoms across the interface is limiting, then we would not be able to explain the low-temperature data for Fe-C to such a high degree as illustrated in Fig. 16. Therefore, an Fe-0.8C-1.0Mn wt% alloy was made and the microstructure and growth rates of pearlite were measured for samples transformed at 958 K and 823 K, consistent to the experiments of Razik *et al* [67]. About 500 g of steel sample was charged in a refractory crucible made of Al_2O_3 (OD 60 mm × ID 52 mm × H 100 mm).

The steel sample in the crucible was melted in a reaction chamber made of a quartz tube equipped with water cooled brass end caps in an induction furnace. Argon gas purified by passing through silica gel and Mg chips heated at 723 K (450 °C), was passed through the reaction chamber during the experiment and the sample solidified by natural cooling. The sample was the sealed in an evacuated quartz tube, homogenised at 1250 °C for 48 h and hot-rolled at 1000 °C to 12 mm thickness and water quenched. The final chemical composition was Fe-0.79C-0.98Mn wt%. Specimens 3 mm diameter and 10 mm length were wire cut for dilatometer experiments (Dilatronic lll, Theta Inc). The heat treatments were conducted in the dilatometer, with the sample austenitised 1100 °C and left for 10 min, cooled to transformation temperature, 823 K and 958 K and finally quenched to room temperature.

Transformation at 958 K led to the classical round pearlite colonies, the shape of which was affected only by the presence of the austenite grain boundaries Fig. 26. However, it is evident that the classical shape gen-

erated by the cooperative growth of ferrite and cementite clearly broke down during transformation at 823 K (Fig. 27). The transmission electron micrograph shown in Fig. 27d was obtained by machining a sample specifically from the spiky transformation product using focused ion-beam milling. It is evident that the cementite and ferrite do not share a common transformation front, with disconnected cementite particles present within the predominantly ferritic matrix. When this happens, the growth rate should decrease because the lack of cooperation would increase the diffusion distances, and with the shapes observed, boundary diffusion at the transformation front would make a smaller contribution since the flux becomes less parallel to the interface.

It could be argued that the spiky transformation product observed for 823 K is in fact bainite. Experiments were therefore done to see whether this non-cooperative growth product results in the surface relief that is typical of bainite, as opposed to diffusional transformation produces that only result in volume changes. Metallographically polished but un-etched samples were heat treated using the dilatometer, and then inspected for surface relief. The sample was austenitised at 1100 °C and left for 10 min, cooled to transformation temperature, 823 K, stayed for 3.6 s, then quenched to room temperature. Hardness indents were used as fiducial marks to correlate surface relief with the same area after very light etching using 2 % nital in ethanol with less than 10 s. Fig. 28 shows with clarity that the only surface relief is from the few plates of bainite that formed during the quench, with neither the spiky nor regular bainite exhibiting any such upheavals.

Table 3 compares our experimental data, derived specifically from isolated, spherical pearlite colonies, using the largest colony method, against those from ref. [67]. There is good agreement for transformation at 958 K but our growth rate for 823 K is larger and more consistent with the cal-

culated values. We are not able to explain this discrepancy at this moment. It is noteworthy that neutron depolarisation experiments [73] gave a pearlite growth rate of $1.19 \times 10^{-7}\,\mathrm{m\,s^{-1}}$ at 953 K in a Fe-0.715C-0.611Mn-0.266Cr-0.347Si wt%, consistent with the present work if the differences in substitutional solute concentrations are neglected.

Table 3: Comparison of measured growth rate [67] against our experimental data.

	958 K	823 K
Measured rate / $\mathrm{m\,s^{-1}}$ [67]	1.63×10^{-7}	9.54×10^{-6}
Measured rate / $\mathrm{m\,s^{-1}}$, current work	1.09×10^{-7}	2.30×10^{-5}
Calculated rate / $\mathrm{m\,s^{-1}}$	1.87×10^{-7}	3.12×10^{-5}

The spiky growth of pearlite was expected by Hillert [38] in his work using limitation of atomic dimension during NPLE mode. The concentration spike of substitutional solute in NPLE mode is also exist in pearlite. The depth of the concentration spike was calculated by D_X/v, where D_X is diffusivity of slow diffuser, and v is growth rate. Hillert analysed that if the depth of the spike D_X/v is less than atomic dimension, the ferrite-austenite interface in pearlite will grow like martensite and the cooperative growth will break down. However, even if all of the reported growth rate, except near A_3 temperature, are having the depth less than 1 Å with volume D_X, the martensitic interface did not observed for those data.

In this work, the depth of concentration spike is calculated with effective diffusivity which is the effective term of volume and boundary diffusion coefficient in mixed diffusion-controlled growth of pearlite.

The calculated depth of concentration spike with three diffusion mech-

anism, volume, boundary and mixed diffusion, are compared in Table. 4 at the temperature of 958 K and 823 K which are taken metallographical analysis. The other two mechanisms gives much lower or higher depth of concentration spike than 1 Å for all temperature. On the other hand, the mixed diffusion-controlled growth mechanism gives the depth of spike an order lower than 1 Å at 823 K and much larger depth at 958 K. The existence of spiky pearlite growth at specific temperature can be perfectly explained by the depth of concentration spike calculated by mixed diffusion mechanism. Thus, the results strongly support the mixed diffusion-controlled growth is the closest mechanism to explain pearlite growth.

Table 4: Comparison of the depth of concentration spike based on mixed diffusion, volume diffusion, and boundary diffusion-controlled growth.

	958 K	823 K
$\frac{D^{\mathrm{Mn}}_{eff}}{v}$ / m	1.77×10^{-8}	3.88×10^{-11}
$\frac{D^{\mathrm{Mn}}_{V}}{v}$ / m	2.09×10^{-13}	1.06×10^{-17}
$\frac{D^{\mathrm{Mn}}_{B}}{v}$ / m	4.68×10^{-6}	3.42×10^{-9}

4.5 Conclusions

It has been possible to find solutions that satisfy local equilibrium at the pearlite transformation front for both the Fe-C and Fe-C-X systems. The method used to achieve this involves independent calculations of growth velocity based on each solute, followed by iteration to achieve the same growth rate irrespective of solute. The method takes into account both boundary and volume diffusion, gives satisfactory closure between theory

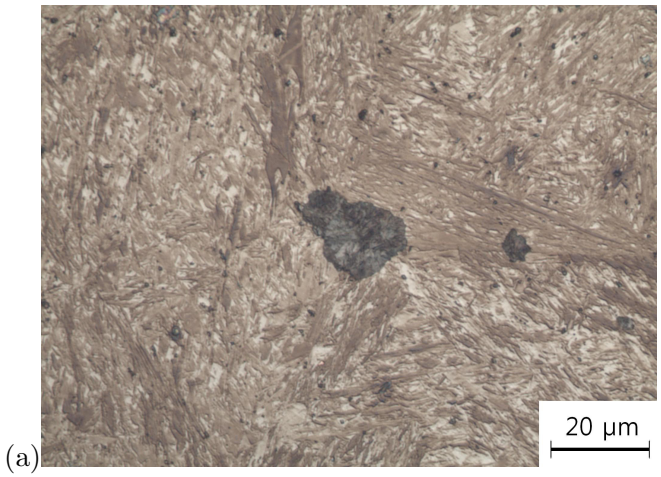

(a)

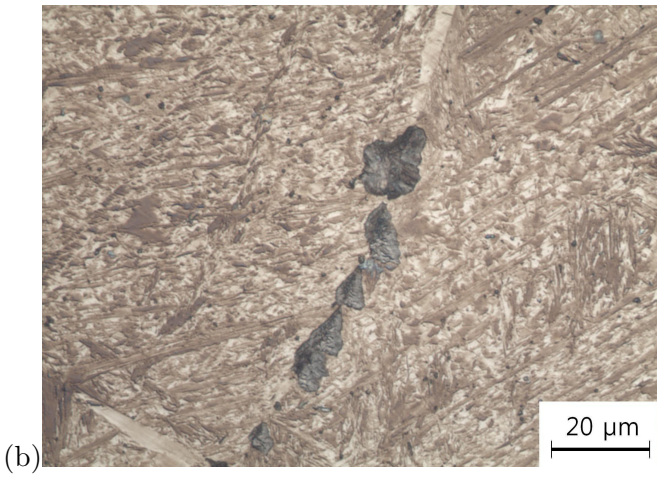

(b)

Figure 26: Microstructure of isothermal transformation at 957 K held for 2 min by optical micrograph. (a) and (b) show spherical shape of typical pearlite morphology.

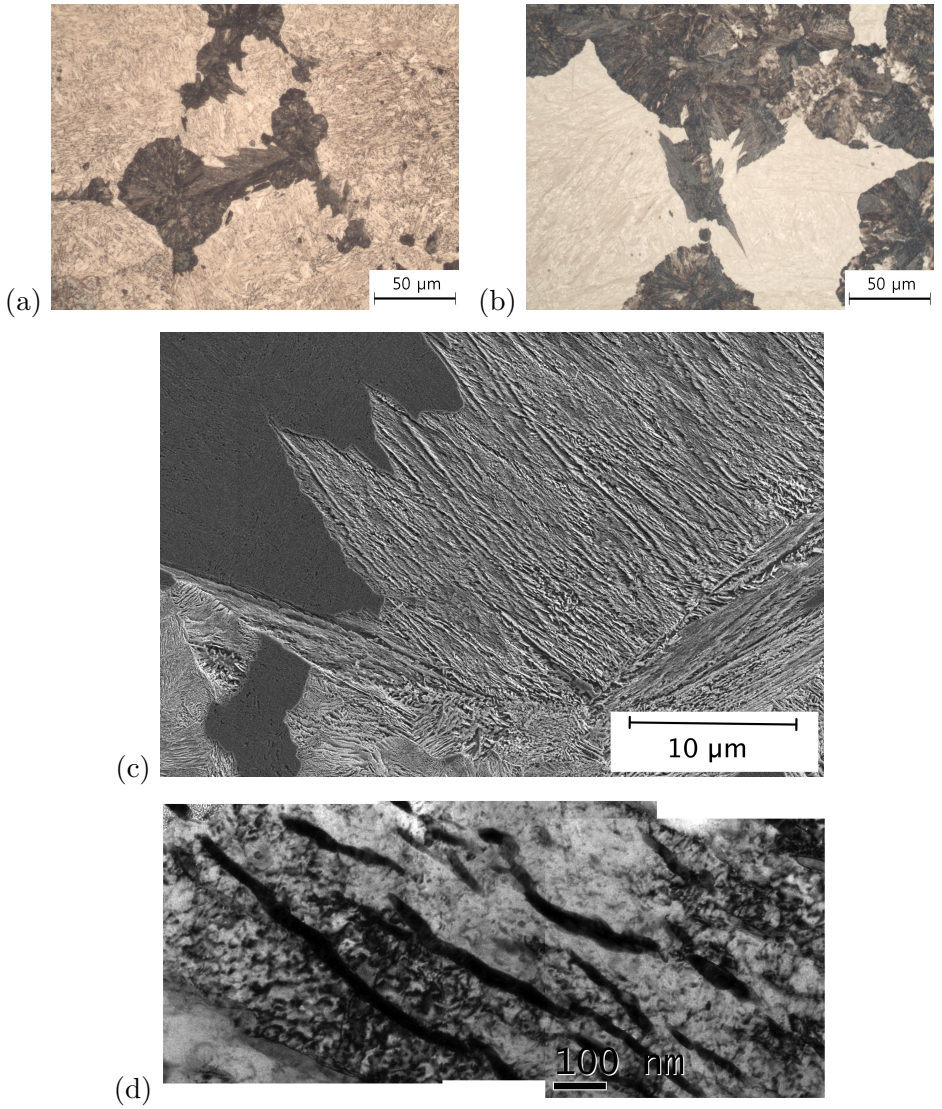

Figure 27: Optical micrographs of isothermal transformation at 823 K held for (a) 3.6 s and (b) 5 s. (c) Scanning electron micrograph (3.6 s). (d) Transmission electron micrograph (3.6 s).

(a)

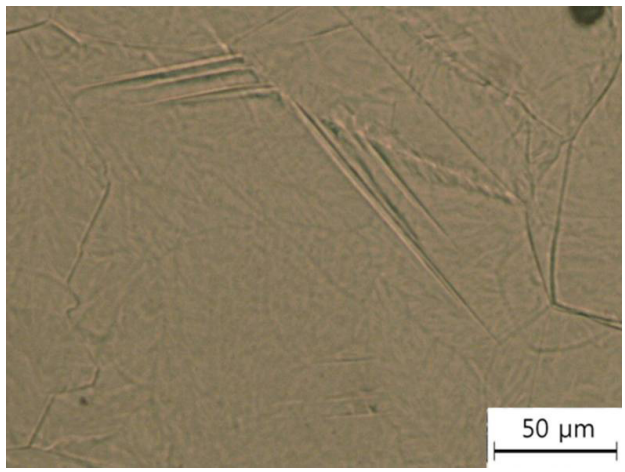

(b)

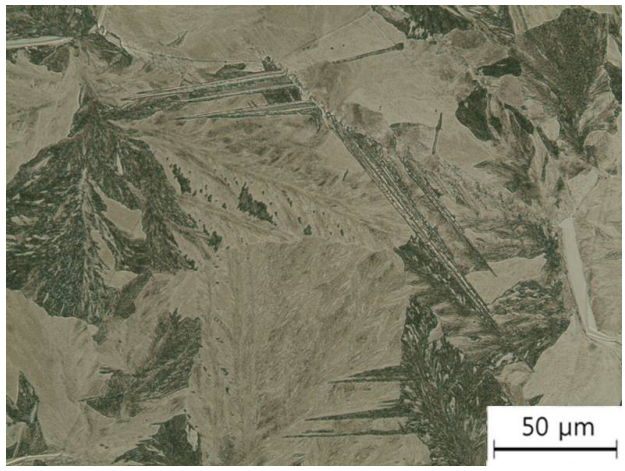

Figure 28: Corresponding images from the surface relief experiments. The dark-etching spiky form of pearlite where the ferrite and cementite do not grow at a common transformation front does not exhibit any surface upheavals. Nor does any of the pearlite. It is only the few plates of lighter-etching bainite that show the surface relief. (a) Unetched sample, (b) after light etching. Samples transformed at 823 K for 3 s.

and experiment. The calculation results of Cr is usually more than an order away from the experimental data, the reason might be raised from the off-diagonal diffusivity. The elements which have low chemical interaction such as nickel and cobalt shows excellent agreement between theory and experiments.

The largest discrepancy between published data on the Fe-Mn-C system and theory exists at the lowest transformation temperature, where we have demonstrated that two forms of pearlite form, one represented by the regular spheroidal colony and the other by a spiky morphology where the cooperation between ferrite and cementite breaks down. In such circumstances, the growth rate equations derived for cementite and ferrite sharing a common transformation front with austenite do not apply. When the growth rate is measured only for the spheroidal colonies of pearlite, even the low temperature data closely approximate theory. The spiky pearlite can be predicted by calculation of the concentration spike depth during the growth whether it is less then atomic distance or not. However, the other mechanisms are impossible to explain the existence of spiky pearlite.

Finally, it has been demonstrated that the spiky transformation product does not lead to the surface relief effect associated with displacive transformations.

5 Analysis of Local Equilibrium Condition During Pearlite Growth

The most important assumptions in PLE and NPLE is the substitutional solute, X, diffuses much slower than the interstitial solute, carbon. However, it was considered as trivial fact even when the former researches dealt with boundary diffusion during pearlite transformation. Fig. 20 shows the diffusivity ratio of carbon to manganese in volume and boundary have different in many orders. As reminding the PLE and NPLE work in the condition of $D_X \ll D_C$, those two local equilibrium modes does not appropriate to apply in mixed diffusion-controlled pearlite transformation.

In the previous chapter, the local equilibrium condition for pearlite transformation was found from two simple constraints, mass conservation and velocity conservation. However, the condition was calculated through the iterative program using Thermo-Calc. Thus the uniqueness of solution or the dependence on diffusivity ratio remain unknown. In this chapter, the local equilibrium condition for pearlite growth will be tested more analytical method to understand its nature.

5.1 Method

Fig. 29 shows a brief Fe-X-C phase diagram where X is the substitutional alloying element. There are five points which are the interface compositions, $c^{\alpha\gamma}$, $c^{\theta\gamma}$, $c^{\gamma\alpha}$ and $c^{\gamma\theta}$, and average composition, $\bar{c}$. Each points can be expressed by carbon and manganese composition as a coordinate in phase diagram. Back to mass conservation condition, the interface compositions

should satisfy below:

$$\frac{c_{\mathrm{X}}^{\theta\gamma}-c_{\mathrm{X}}^{\alpha\gamma}}{c_{\mathrm{C}}^{\theta\gamma}-c_{\mathrm{C}}^{\alpha\gamma}}=\frac{\bar{c}_{\mathrm{X}}-c_{\mathrm{X}}^{\alpha\gamma}}{\bar{c}_{\mathrm{C}}-c_{\mathrm{C}}^{\alpha\gamma}}=\frac{c_{\mathrm{X}}^{\theta\gamma}-\bar{c}_{\mathrm{X}}}{c_{\mathrm{C}}^{\theta\gamma}-\bar{c}_{\mathrm{C}}} \tag{58}$$

where the subscript X and C denote each solutes. This condition makes possible that pearlite consume the whole system. As a result of lever rule, points $c^{\theta\gamma}$ and $c^{\alpha\gamma}$ literally move like lever having pivot point $\bar{c}$.

The other condition, the velocity conservation, can give the relationship between 'the lever' and the diffusivity ratio. It can be equated:

$$\begin{aligned}\frac{D_{\mathrm{C}}}{D_{\mathrm{X}}}=\frac{R_{\mathrm{X}}}{R_{\mathrm{C}}}&=\frac{c_{\mathrm{X}}^{\gamma\alpha}-c_{\mathrm{X}}^{\gamma\theta}}{c_{\mathrm{X}}^{\theta\gamma}-c_{\mathrm{X}}^{\alpha\gamma}}\cdot\frac{c_{\mathrm{C}}^{\theta\gamma}-c_{\mathrm{C}}^{\alpha\gamma}}{c_{\mathrm{C}}^{\gamma\alpha}-c_{\mathrm{C}}^{\gamma\theta}}=\frac{c_{\mathrm{X}}^{\gamma\alpha}-c_{\mathrm{X}}^{\gamma\theta}}{c_{\mathrm{C}}^{\gamma\alpha}-c_{\mathrm{C}}^{\gamma\theta}}\cdot\frac{c_{\mathrm{C}}^{\theta\gamma}-c_{\mathrm{C}}^{\alpha\gamma}}{c_{\mathrm{X}}^{\theta\gamma}-c_{\mathrm{X}}^{\alpha\gamma}}\\&=\frac{\text{slope of line }\overline{c^{\gamma\theta}c^{\gamma\alpha}}}{\text{slope of line }\overline{c^{\alpha\gamma}c^{\theta\gamma}}}\end{aligned} \tag{59}$$

With the fact that the tie-line connect the points at α/γ and θ/γ interfaces, it is possible to test the unique existence of interface composition for given diffusivity ratio. Let's assume the situation that the compositions $c^{\alpha\gamma}$ or $c^{\theta\gamma}$ move towards x-axis, then the points $c^{\gamma\alpha}$ or $c^{\gamma\theta}$ will follow the direction to x-axis. In contrast, if the compositions of product phases changes away from the x-axis then connected interface compositions will show same behaviour. It is obvious because the tie-lie is the line between free energy surfaces of two different phases.

Now, it is known that the compositions of product phases follows the lever rule, for example, $c^{\theta\gamma}$ goes to downward, then it cause the upward compensation of $c^{\alpha\gamma}$. Moreover, this changes also affect on the interface

composition at austenite side. As continuing previous example, downward movement of $c^{\theta\gamma}$ cause same change to $c^{\gamma\theta}$ and upward movement of both $c^{\alpha\gamma}$ and $c^{\gamma\alpha}$. Finally, the slope of line $\overline{c^{\alpha\gamma}c^{\theta\gamma}}$ will decrease but the slope of line $\overline{c^{\gamma\theta}c^{\gamma\alpha}}$ will increase. Combining this results with equation 59, it is noticeable that diffusivity ratio $D_{\mathrm{C}}/D_{\mathrm{X}}$ is increasing as $c_{\mathrm{X}}^{\theta\gamma}$ goes to 0. Thus, it is possible to describe the diffusivity ratio as a function of X composition in cementite:

$$\frac{D_{\mathrm{C}}}{D_{\mathrm{X}}} = \frac{R_{\mathrm{X}}}{R_{\mathrm{C}}} = f(c_{\mathrm{X}}^{\theta\gamma}) \tag{60}$$

This is based on the fact that the composition of carbon in cementite, $c_{\mathrm{C}}^{\theta\gamma}$, is always constant. The most important property of this function $f(c_{\mathrm{X}}^{\theta\gamma})$ is shown in previous example with decreasing $c_{\mathrm{X}}^{\theta\gamma}$: **The function $f(c_{\mathrm{X}}^{\theta\gamma})$ is monotonic decreasing function** or it can be described as:

$$\frac{\mathrm{d}\, f(c_{\mathrm{X}}^{\theta\gamma})}{\mathrm{d}\, c_{\mathrm{X}}^{\theta\gamma}} < 0 \tag{61}$$

As a result, the local equilibrium condition is unique for given diffusivity ratio and mean composition. When the ratio $D_{\mathrm{C}}/D_{\mathrm{X}}$ goes to infinite, it is associated with the local equilibrium condition:

$$\text{slope of line } \overline{c^{\gamma\theta}c^{\gamma\alpha}} = \infty \tag{62}$$

or

$$\text{slope of line } \overline{c^{\alpha\gamma}c^{\theta\gamma}} = 0 \tag{63}$$

More specific analysis on this conditions will be dealt in next section.

5.2 Analysis

The similar analysis was done by Coates [62] but it was only single phase transformation. In pearlite transformation, the previous two conditions, equation 58 and 59 show the increase of complexness by coupling two phase transformation at the same time. The idea of interface composition (IC) contour was suggested by Coates [62] and it is also applied to current analysis of pearlite. The IC contour, which is the series of average compositions sharing the same interface composition, is usually a curve except the case $D_{\mathrm{C}}/D_{\mathrm{X}}$ is unity in the work of Coates. The IC contour during the pearlite transformation, however, has straight line for all possible diffusivity ratio and the line is $\overline{c^{\alpha\gamma}c^{\theta\gamma}}$. Also, during single phase transformation, a single tie-line can have infinite number of IC contours which they have different diffusivity ratio to each other. IC contour during pearlite transformation, unlikely to previous case, connected to two different tie-line which are in $\alpha+\gamma$ and $\gamma+\theta$ phase field (Fig. 33). Therefore, the set of tie-lines will have an unique IC contour. Instead of tie-lines, it is possible that to group the IC contours which pass the common mean composition as shown in Fig. 33. The growth rate is decided by the position of mean composition on IC contour that makes difference of phase fraction in Eq. 41. Thus, the term related to interface compositions maintains constant on the arbitrary IC contour, and the terms $S_\alpha S_\theta$ which are related to phase fraction decide the growth rate. Also, the diffusivity ratio change implies that interface composition term R_{i} in Eq. 59 follows its ratio, thus, the difference between diffusivity ratio 1000 and 10000 in Fig. 32 looks like negligible but it cause miscalculation of growth rate. In conclusion, looking for precise R_{i} for given diffusivity ratio is essential to predict the growth rate of pearlite.

As shown in Eq. 62, two conditions are possible to exist during pearlite transformation. When their IC contours and related tie-lines are plotted on the phase diagram (Fig. 34), it can be distinguished by the existence of partitioning between ferrite and cementite. The previous research of Hillert [38] focused on the relationship between ferrite-austenite and cementite-austenite partitioning, however, in the local equilibrium condition deduced from Eq. 41, the partitioning between ferrite and cementite is more important. It is noticeable that the upper mean composition in Fig. 34 which has higher Mn and lower C composition always produces the pearlite which has partitioning of element X between ferrite and cementite as diffusivity ratio gets larger and larger. On the contrary, the lower mean composition which has lower Mn and higher C composition loses the X partitioning between ferrite and cementite when the $D_{\mathrm{C}}/D_{\mathrm{X}}$ increases to infinite. Clearly, the two different mean composition in Fig. 34 have different mode of transformation, PLE and NPLE. Combining this result with Eq. 62 and 63, it can be deduced that the mean composition which follows PLE condition during pearlite transformation is equivalent to Eq. 62 and NPLE is Eq. 63. In this work, instead of calculation of PLE-NPLE boundary, the condition for boundary is suggested: at the boundary of PLE and NPLE in pearlite transformation, both of

$$\text{slope of line } \overline{c^{\gamma\theta}c^{\gamma\alpha}} = \infty$$
$$\text{slope of line } \overline{c^{\alpha\gamma}c^{\theta\gamma}} = 0$$

will be satisfied simultaneously when $D_{\mathrm{C}}/D_{\mathrm{X}} = \infty$. The most important point of this result is that pearlite transformation in the green area of Fig. 14 can be understood with breaking the classical LE conditions and use new solutions for diffusion equation. Although the solutions are the result

of simplified system, the result is well supported by the experiment.

Calculation of growth rate is now a bit more complicate than the single phase transformation, constructing interface velocity (IV) contour is consuming too much time. Therefore, in this work, the IV contour that was shown in Coates' work [62] does not reconstructed for pearlite transformation.

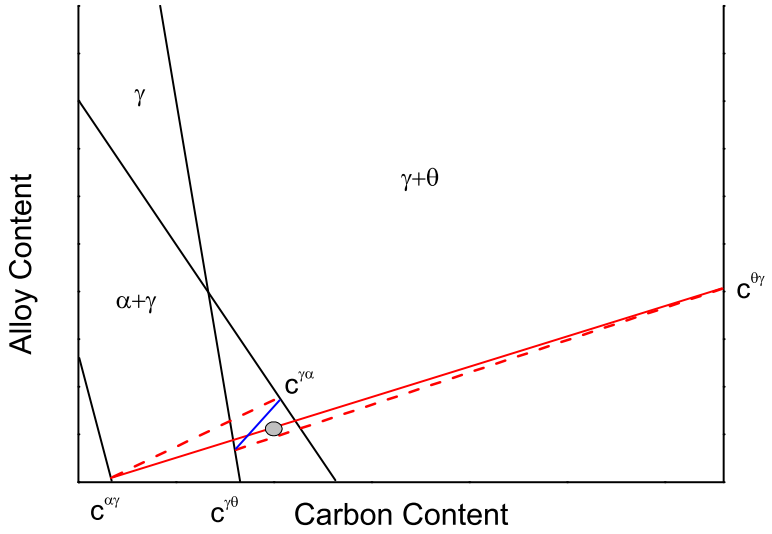

Figure 29: Related interface compositions in Fe-X-C phase diagram. Solid red line is the line passing through the mean, ferrite and cementite compositions. The red broken lines are acting tie-lines. The blue line is connecting austenite interface compositions.

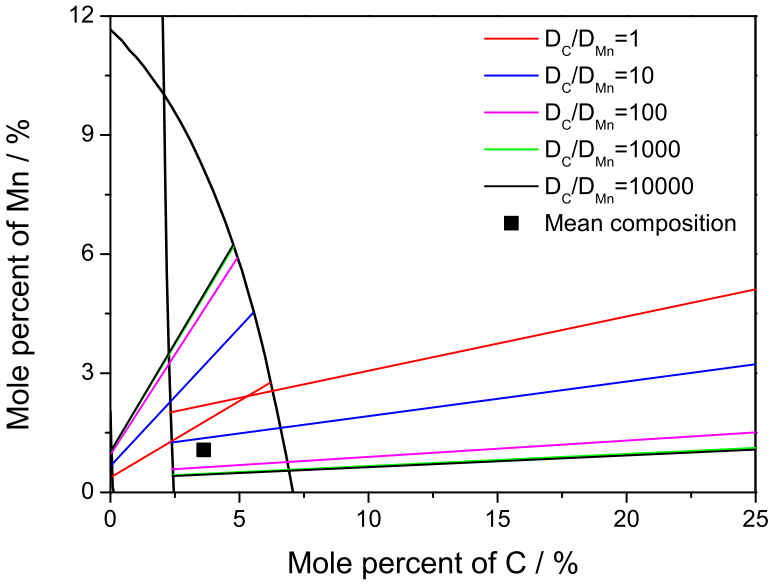

Figure 30: Change of tie-line when the compositions $c^{\theta\gamma}$ and $c^{\alpha\gamma}$ are changed in Fe-Mn-C ternary system. The tie-lines are calculated for pearlite transformation with various diffusivity ratio.

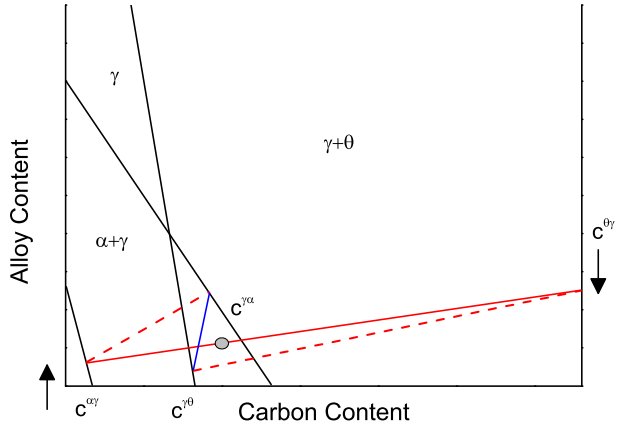

(a)

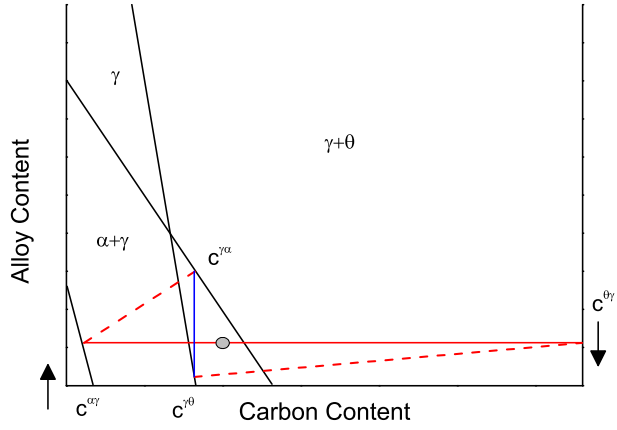

(b)

Figure 31: Change of interface compositions caused by movement of $c^{\theta\gamma}$ and $c^{\alpha\gamma}$. (a)Positions after taking lower composition of $c^{\theta\gamma}$ than Fig.30 and (b)the compositions at the limit

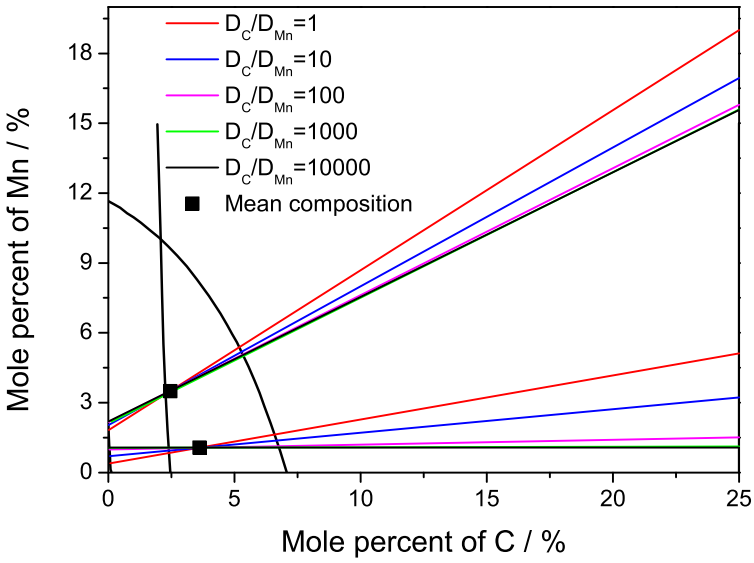

Figure 32: IC contours of two different mean composition for various diffusivity ratio.

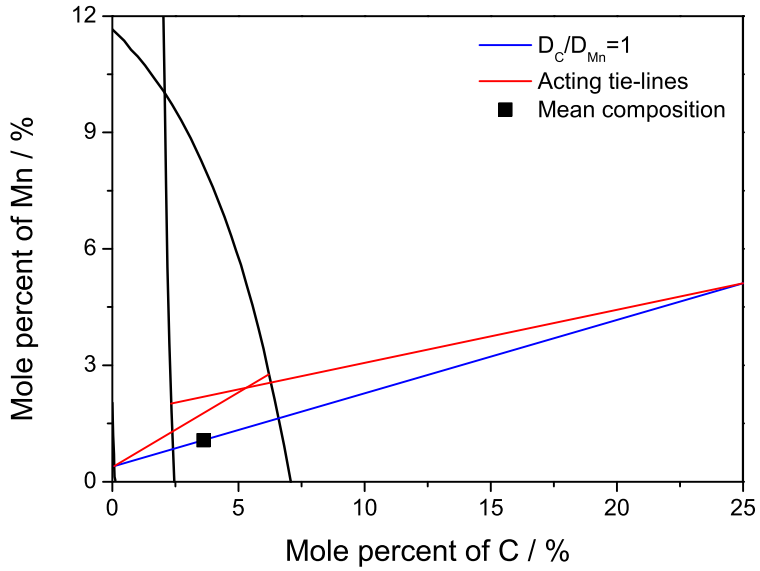

Figure 33: IC contour and related acting tie-lines calculated by Thermo-calc[41].

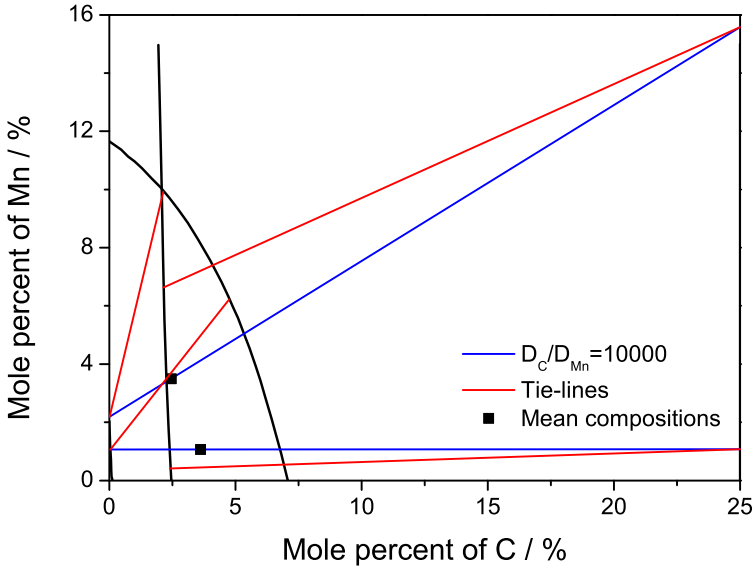

Figure 34: Acting tie-lines and IC contours for PLE and NPLE condition at high diffusivity ratio.

6 Conclusions and Future Work

6.1 Conclusions

In present thesis, the mixed diffusion-controlled growth of pearlite is studied for the Fe-C and Fe-X-C ternary system. To solve the diffusion equation, the system is modified for simplicity. This is because to avoid over fitting of the parameters. In [9], too many parameters gave a result that boundary diffusion is harder path than lattice diffusion. The solution in this thesis gives a reasonable value of activation energy for carbon boundary diffusion comparing with volume diffusion and it describes well for the other experimental results which are not used to deduce boundary diffusion coefficient. It has been shown that the flux ratio of boundary to volume for various temperatures. The results show that the flux of boundary diffusion is usually dominant for most of temperature range except near the eutectoid temperature.

For Fe-X-C ternary system, previous researches [38, 11] suggested the conditions to maintain local equilibrium condition at interphase boundaries, however, they were not enough to explain the pearlite transformation. Moreover, the boundary diffusion coefficient reduces the diffusivity ratio between carbon and substitutional solute and making differences from classical PLE and NPLE condition. The remaining problems of the mixed diffusion for ternary system were solved based on two principles. One is mass conservation of solute during austenite to pearlite transformation, and second is that the pearlite growth rate must have same results without which solutes is used for calculating the growth rate. With series of iterative calculations with Thermo-Calc, this thesis makes possible to get precise interface composition term R which satisfying local equilibrium. The results also supported by reported analytical electron microscopy data.

At low temperatures, the loss of cooperative growth in pearlite is observed. This phenomenon is analysed using various metallographic techniques including a surface relief experiment. As a result, it is determined that the spiky form of pearlite has no surface relief effect thus it is the product of diffusional transformation. It is supposed that the broken cementite causes longer diffusion distance for the solutes and slows down the growth rate. This broken cementite was predicted by Hillert [38] from limitation of diffusion distance D_{X}/v, but volume and boundary diffusion controlled growth gave discrepancies to experimental results. The mixed diffusion equation is strongly supported by this limitation and it gives a reasonable explanation for existence of spiky pearlite at low temperature.

The local equilibrium condition suggested in this thesis to describe pearlite transformation is analysed with assuming various diffusivity ratio and compared to single phase transformation. It is shown that the local equilibrium condition exists uniquely for given mean composition and diffusivity ratio. Also, PLE and NPLE in pearlite transformation is now focusing on partitioning between ferrite and cementite.

6.2 Future Work

Work in this thesis suggested the description of pearlite using mixed diffusion controlled growth. The mixed diffusion model and experiment agrees well for both Fe-C and Fe-X-C systems. Remaining difficulty in ternary system is how to take account the chemical interactions between carbon and substitutional solute fluxes. Because the boundary diffusion data is lacking, there are a few options for solving mixed diffusion equation. The most promising solution is constructing database for boundary diffusion coefficient with combination of solutes with experiments. Multi-scale modelling

such as combination of first-Principles calculations and molecular dynamics and etc. can be a good alternative way to building boundary diffusivity database [80, 81].

As shown in present thesis, the elements which has small interaction with carbon (Co, Ni, etc.) have good agreement with experiments without considering above problems unlike Cr. Therefore, expansion of mixed diffusion model to quaternary system can have good starting point with those elements before the boundary diffusion database have enough information.

The spiky pearlite has not been modelled in this thesis because its shape loses the symmetry of classical pearlite. Thus the successful modelling of this spiky pearlite could give a description the transition of diffusional to displacive transformation.

7 Appendix

7.1 Mathematica source code

Mathematica source code is programmed to find S_C/S by equating Eq. 45 and experimental pearlite growth rate of Frye *et al.* [74]

```
Dv=0.000015*Exp[-135000/(8.314472*T)]
Dc=5.004338714*10^-3*Exp[-132877.8/(8.3144*T)]
x=1/(162034000-166210.00398*T)
f[S_]:=(  (Dv+(6Dc  2.5)/(10^10  S))   (1-Sc/S))/S
f'[S]
Solve[((0.000015`  E^(-16236.749609596374`/T)
    +(7.506508071`*^-12  E^(-15981.646300394497`/T))/x)
    al)/x^2-((0.000015`  E^(-16236.749609596374`/T)
    +(7.506508071`*^-12  E^(-15981.646300394497`/T))/x)
    (1-al))/x^2+((0.`\[VeryThinSpace
    ]-(7.506508071`*^-12  E^(-15981.646300394497`/T))/x
    ^2)  (1-al))/x==0,al]
```

7.2 TC-API source code

The TC-API module is used to find local equilibrium condition in Fe-X-C ternary system with C language. Related header file and dynamic-link library (DLL) file are given by Thermo-Calc software [41].

This source code needs Thermo-Calc software in the executing computer.

```
/* Calculates an equilibrium in the Fe-Mn-C system and
    retrieves certain quantities. */



#include <stdio.h>
#include <string.h>


#include "tcapi.h"

int main( int argc, char **argv)
{
  char *line, *sub, *xsub, *fbsub, *bfsub, *cfsub, *
     database;
  double value,c_cgt,c_ctg,c_cga,c_cag,c_mngt,c_mntg,
     c_mnga,c_mnag,eng_err,eng_err2,abs_eng,abs_eng2;
  double temp_c1,temp_mn1,temp_mn2,temp_c,temp_mn;
  double c_min,mn_min,distance,temperature;
  double ratio,alpha_c,alpha_mn;

  //Now automation of finding proper ratio of
     effective diffusivity is updating (11/05/2013)
  double target;
  char error[80];
  int ierr;

  sub="MN";
```

```
xsub="X(MN)";
fbsub="X(FCC_A1,MN)";
bfsub="X(BCC_A2,MN)";
cfsub="X(CEMENTITE,MN)";
database="SSOL4";

c_min=0.0246;//  Hut:0.0246,1.08Mn:0.036136, 1.8Mn
    :0.031285, 1.4CR:0.03742
mn_min=0.035;//  Hut:0.035,1.08Mn:0.010665, 1.8Mn
    :0.017843, 1.4CR:0.01458

/* fcc-cem mean composition */

temp_mn=0.1487;//  Hut:0.1458, 1.08Mn:0.0099, 1.8Mn
    :0.048
temp_c=0.23002;//   Hut:0.23002, 1.08Mn:0.22, 1.8Mn
    :0.22
temperature=900;
//target effective diffusivity
target=1000;

  /* Making Roop to find the point */
abs_eng=1;
temp_mn1=0.05; // 1.08Mn&1.8Mn:0.03
temp_c1=0.01; // 1.08Mn&1.8Mn:0.01

do{     /* Added in 11/05/2013 */
/* Set initial gamma-cementite information */
```

```
/* Initialize the system */
tc_init_root();
ierr=0;
if ( tc_error(&ierr,error,sizeof(error)) ) {
  fprintf(stdout,"error: %d : %s\n",ierr,error);
  tc_reset_error();
}


/* Open database */
tc_open_database(database);
ierr=0;
if ( tc_error(&ierr,error,sizeof(error)) ) {
  fprintf(stdout,"error: %d : %s\n",ierr,error);
  tc_reset_error();
}


/* Select the elements */
line="FE";
tc_element_select(line);
ierr=0;
if ( tc_error(&ierr,error,sizeof(error)) ) {
  fprintf(stdout,"error: %d : %s\n",ierr,error);
  tc_reset_error();
}
```

```
tc_element_select(sub);
ierr=0;
if ( tc_error(&ierr,error,sizeof(error)) ) {
  fprintf(stdout,"error: %d : %s\n",ierr,error);
  tc_reset_error();
}

line="C";
tc_element_select(line);
ierr=0;
if ( tc_error(&ierr,error,sizeof(error)) ) {
  fprintf(stdout,"error: %d : %s\n",ierr,error);
  tc_reset_error();
}


/* Reject all phases */
line="*";
tc_phase_reject(line);
ierr=0;
if ( tc_error(&ierr,error,sizeof(error)) ) {
  fprintf(stdout,"error: %d : %s\n",ierr,error);
  tc_reset_error();
}


/* Restore phases */
line="FCC_A1";
```

```
tc_phase_select(line);
ierr=0;
if ( tc_error(&ierr,error,sizeof(error)) ) {
  fprintf(stdout,"error: %d : %s\n",ierr,error);
  tc_reset_error();
}

line="CEMENTITE";
tc_phase_select(line);
ierr=0;
if ( tc_error(&ierr,error,sizeof(error)) ) {
  fprintf(stdout,"error: %d : %s\n",ierr,error);
  tc_reset_error();
}


/* Get the data from the database */
tc_get_data();
ierr=0;
if ( tc_error(&ierr,error,sizeof(error)) ) {
  fprintf(stdout,"error: %d : %s\n",ierr,error);
  tc_reset_error();
}


/* Set the necessary conditions */
value=temp_mn;
tc_set_condition(xsub,value);
```

```
ierr=0;
if ( tc_error(&ierr,error,sizeof(error)) ) {
  fprintf(stdout,"error: %d : %s\n",ierr,error);
  tc_reset_error();
}


line="X(C)";   value=temp_c;
tc_set_condition(line,value);
ierr=0;
if ( tc_error(&ierr,error,sizeof(error)) ) {
  fprintf(stdout,"error: %d : %s\n",ierr,error);
  tc_reset_error();
}


line="T";      value=temperature;
tc_set_condition(line,value);
ierr=0;
if ( tc_error(&ierr,error,sizeof(error)) ) {
  fprintf(stdout,"error: %d : %s\n",ierr,error);
  tc_reset_error();
}


line="N";      value=1;
tc_set_condition(line,value);
ierr=0;
```

```
if ( tc_error(&ierr,error,sizeof(error)) ) {
  fprintf(stdout,"error: %d : %s\n",ierr,error);
  tc_reset_error();
}


line="P";       value=101325;
tc_set_condition(line,value);
ierr=0;
if ( tc_error(&ierr,error,sizeof(error)) ) {
  fprintf(stdout,"error: %d : %s\n",ierr,error);
  tc_reset_error();
}


/* Compute the equilibrium */

tc_compute_equilibrium();
ierr=0;
if ( tc_error(&ierr,error,sizeof(error)) ) {
  fprintf(stdout,"error: %d : %s\n",ierr,error);
  tc_reset_error();
}


/* Check the number of Phases */
/* tc_stable_phases(phs,value);
if(value!=2){
```

```
        fprintf(stdout,"Reset FCC-CEM component
            !!!!");
        tc_deinit();
}
*/



/* Retrieve the desired value */

value=tc_get_value(fbsub);
ierr=0;
if ( tc_error(&ierr,error,sizeof(error)) ) {
  fprintf(stdout,"error: %d : %s\n",ierr,error);
  tc_reset_error();
}
c_mngt=value;

value=tc_get_value(cfsub);
ierr=0;
if ( tc_error(&ierr,error,sizeof(error)) ) {
  fprintf(stdout,"error: %d : %s\n",ierr,error);
  tc_reset_error();
}
c_mntg=value;

line="X(FCC_A1,C)";
value=tc_get_value(line);
```

```
ierr=0;
if ( tc_error(&ierr,error,sizeof(error)) ) {
  fprintf(stdout,"error: %d : %s\n",ierr,error);
  tc_reset_error();
}
c_cgt=value;

line="X(CEMENTITE,C)";
value=tc_get_value(line);
ierr=0;
if ( tc_error(&ierr,error,sizeof(error)) ) {
  fprintf(stdout,"error: %d : %s\n",ierr,error);
  tc_reset_error();
}
c_ctg=value;

tc_deinit();


/* Find gamma-alpha composition */

/* Initialize the system */

tc_init_root();
ierr=0;
if ( tc_error(&ierr,error,sizeof(error)) ) {
  fprintf(stdout,"error: %d : %s\n",ierr,error);
  tc_reset_error();
```

```
}


/* Open database */
tc_open_database(database);
ierr=0;
if ( tc_error(&ierr,error,sizeof(error)) ) {
  fprintf(stdout,"error: %d : %s\n",ierr,error);
  tc_reset_error();
}


/* Select the elements */
line="FE";
tc_element_select(line);
ierr=0;
if ( tc_error(&ierr,error,sizeof(error)) ) {
  fprintf(stdout,"error: %d : %s\n",ierr,error);
  tc_reset_error();
}

tc_element_select(sub);
ierr=0;
if ( tc_error(&ierr,error,sizeof(error)) ) {
  fprintf(stdout,"error: %d : %s\n",ierr,error);
  tc_reset_error();
}
```

```
line="C";
tc_element_select(line);
ierr=0;
if ( tc_error(&ierr,error,sizeof(error)) ) {
  fprintf(stdout,"error: %d : %s\n",ierr,error);
  tc_reset_error();
}


/* Reject all phases */
line="*";
tc_phase_reject(line);
ierr=0;
if ( tc_error(&ierr,error,sizeof(error)) ) {
  fprintf(stdout,"error: %d : %s\n",ierr,error);
  tc_reset_error();
}


/* Restore phases */
line="FCC_A1";
tc_phase_select(line);
ierr=0;
if ( tc_error(&ierr,error,sizeof(error)) ) {
  fprintf(stdout,"error: %d : %s\n",ierr,error);
  tc_reset_error();
}
```

```
line="BCC_A2";
tc_phase_select(line);
ierr=0;
if ( tc_error(&ierr,error,sizeof(error)) ) {
  fprintf(stdout,"error: %d : %s\n",ierr,error);
  tc_reset_error();
}


/* Get the data from the database */
tc_get_data();
ierr=0;
if ( tc_error(&ierr,error,sizeof(error)) ) {
  fprintf(stdout,"error: %d : %s\n",ierr,error);
  tc_reset_error();
}
abs_eng=0.1; //abs_eng initialization.
while(abs_eng>1E-7){

/* Set the necessary conditions */
value=temp_mn1;
tc_set_condition(xsub,value);
ierr=0;
if ( tc_error(&ierr,error,sizeof(error)) ) {
  fprintf(stdout,"error: %d : %s\n",ierr,error);
  tc_reset_error();
}
```

```
line="X(C)";   value=temp_c1;
tc_set_condition(line,value);
ierr=0;
if ( tc_error(&ierr,error,sizeof(error)) ) {
  fprintf(stdout,"error: %d : %s\n",ierr,error);
  tc_reset_error();
}


line="T";      value=temperature;
tc_set_condition(line,value);
ierr=0;
if ( tc_error(&ierr,error,sizeof(error)) ) {
  fprintf(stdout,"error: %d : %s\n",ierr,error);
  tc_reset_error();
}


line="N";      value=1;
tc_set_condition(line,value);
ierr=0;
if ( tc_error(&ierr,error,sizeof(error)) ) {
  fprintf(stdout,"error: %d : %s\n",ierr,error);
  tc_reset_error();
}
```

```
line="P";       value=101325;
tc_set_condition(line,value);
ierr=0;
if ( tc_error(&ierr,error,sizeof(error)) ) {
  fprintf(stdout,"error: %d : %s\n",ierr,error);
  tc_reset_error();
}


/* Compute the equilibrium */

tc_compute_equilibrium();
ierr=0;
if ( tc_error(&ierr,error,sizeof(error)) ) {
  fprintf(stdout,"error: %d : %s\n",ierr,error);
  tc_reset_error();
}


/* Check the number of Phases */
/* tc_stable_phases(phs,value);
if(value!=2){
        fprintf(stdout,"Reset FCC-CEM component
            !!!!");
        tc_deinit();
}
*/
```

```
/* Retrieve the desired value */

value=tc_get_value(fbsub);
ierr=0;
if ( tc_error(&ierr,error,sizeof(error)) ) {
  fprintf(stdout,"error: %d : %s\n",ierr,error);
  tc_reset_error();
}
c_mnga=value;

value=tc_get_value(bfsub);
ierr=0;
if ( tc_error(&ierr,error,sizeof(error)) ) {
  fprintf(stdout,"error: %d : %s\n",ierr,error);
  tc_reset_error();
}
c_mnag=value;

line="X(FCC_A1,C)";
value=tc_get_value(line);
ierr=0;
if ( tc_error(&ierr,error,sizeof(error)) ) {
  fprintf(stdout,"error: %d : %s\n",ierr,error);
  tc_reset_error();
}
c_cga=value;
```

```
line="X(BCC_A2,C)";
value=tc_get_value(line);
ierr=0;
if ( tc_error(&ierr,error,sizeof(error)) ) {
  fprintf(stdout,"error: %d : %s\n",ierr,error);
  tc_reset_error();
}
c_cag=value;

distance=(c_mntg-mn_min)/(c_ctg-c_min);

eng_err=distance*c_cag+mn_min-distance*c_min-c_mnag;

fprintf(stdout,"eng_err : %g\r",eng_err);

if(eng_err<0){
        abs_eng=eng_err*-1;
        if(abs_eng>1e-4){
        temp_mn2=temp_mn1;
        temp_mn1=temp_mn1-0.0001;
        }
        else if(abs_eng>1e-5){
        temp_mn2=temp_mn1;
        temp_mn1=temp_mn1-0.00001;
        }
        else if(abs_eng>1e-6){
        temp_mn2=temp_mn1;
```

```
            temp_mn1=temp_mn1-0.000001;
            }
            else {
            temp_mn2=temp_mn1;
            temp_mn1=temp_mn1-0.0000001;
            }
  }
  else if(eng_err>0){
            abs_eng=eng_err;
            if(abs_eng>1e-4){
            temp_mn2=temp_mn1;
            temp_mn1=temp_mn1+0.0001;
            }
            else if(abs_eng>1e-5){
            temp_mn2=temp_mn1;
            temp_mn1=temp_mn1+0.00001;
            }
            else if(abs_eng>1e-6){
            temp_mn2=temp_mn1;
            temp_mn1=temp_mn1+0.000001;
            }
            else {
            temp_mn2=temp_mn1;
            temp_mn1=temp_mn1+0.0000001;
            }
  }
//    fprintf(stdout,"%g\n",eng_err);
 }
```

```
// distance=(c_mntg-mn_min)/(c_ctg-c_min);

// eng_err=distance*c_cag+mn_min-distance*c_min-c_mnag
   ;


 /* Get final results */
 fprintf(stdout,"\n");

 alpha_c=(c_cga-c_cgt)/(c_ctg-c_cag);
 alpha_mn=(c_mnga-c_mngt)/(c_mntg-c_mnag);
 ratio=alpha_mn/alpha_c;
 eng_err2=target-ratio;
 if(ratio<0){
          fprintf(stdout,"ratio is less than zero!\n");
          break;
 }
 if(eng_err2<0){
          temp_mn=temp_mn+0.00001;//1.08Mn:+0.00001
          abs_eng2=-1.0*eng_err2;
 }
 else{
          temp_mn=temp_mn-0.00001;//1.08Mn:-0.00001
          abs_eng2=eng_err2;
 }
 fprintf(stdout,"distance to target : %f\n",abs_eng2);
 }while(abs_eng2>0.05*target);
```

```
//
  fprintf(stdout,"%g\n",eng_err);
  fprintf(stdout,"test Mn : %.10g\n",temp_mn2);
  fprintf(stdout,"X(FCC_BCC,C) : %.10g\n",c_cga);
  fprintf(stdout,"X(FCC_CEM,C) : %.10g\n",c_cgt);
  fprintf(stdout,"X(CEM_FCC,C) : %.10g\n",c_ctg);
  fprintf(stdout,"X(BCC_FCC,C) : %.10g\n",c_cag);
  fprintf(stdout,"X(FCC_BCC,Mn) : %.10g\n",c_mnga);
  fprintf(stdout,"X(FCC_CEM,Mn) : %.10g\n",c_mngt);
  fprintf(stdout,"X(CEM_FCC,Mn) : %.10g\n",c_mntg);
  fprintf(stdout,"X(BCC_FCC,Mn) : %.10g\n",c_mnag);
  fprintf(stdout,"Diffusivity ratio : %5g\n",ratio);

   tc_deinit();
}
```

References

[1] M. Hillert. The formation of pearlite. In V. F. Zackay and H. I. Aaronson, editors, *Decomposition of austenite by diffusional processes*, pages 197–237, New York, USA, 1962. Interscience.

[2] C. Zener. Kinetics of the Decomposition of Austenite. *Trans. AIME*, 167:550–595, 1946.

[3] M. Hillert. The role of interfacial energy during solid state phase transformations. *Jernkontorets Annaler*, 141:757–789, 1957.

[4] M. Hillert. *The Mechanism of Phase Transformations in Crystalline Solids*. Institute of Metals, London, 1969.

[5] N. Ridley. The Pearlite Transformation. In A. R. Marder and J I Goldstein, editors, *Phase Transformations in Ferrous Alloys*, pages 201–236. TMS-AIME, Warrendale, PA, 1984.

[6] J. W. Christian. *The Theory of Transformations in Metals and Alloys*, volume Part. 1. Pergamon Press, Oxford, U. K., 3rd edition edition, 2003.

[7] B. E. Sundquist. The Edgewise Growth of Pearlite. *Acta Metallurgica*, 16(12):1413–1427, 1968.

[8] M. Hillert. On Theories of Growth During Discontinuous Precipitation. *Metallurgical Transactions*, 3(11):2729–2741, November 1972.

[9] K. Hashiguchi and J. S. Kirkaldy. Pearlite growth by combined volume and phase boundary diffusion. *Scandinavian Journal of Metallurgy*, 13(4):240–248, 1984.

[10] A. S. Pandit and H. K. D. H. Bhadeshia. Mixed Diffusion-Controlled Growth of Pearlite in Binary Steel. *Proceedings of the Royal Society a-Mathematical Physical and Engineering Sciences*, 467(2126):508–521, 2011.

[11] A. S. Pandit and H. K. D. H. Bhadeshia. Diffusion-Controlled Growth of Pearlite in Ternary Steels. *Proceedings of the Royal Society a-Mathematical Physical and Engineering Sciences*, 467(2134):2948–2961, 2011.

[12] K. Nakajima, M. Apel, and I. Steinbach. The role of carbon diffusion in ferrite on the kinetics of cooperative growth of pearlite: A multi-phase field study. *Acta Materialia*, 54(14):3665–3672, August 2006.

[13] I. Steinbach and M. Plapp. Pearlite revisited. *Continuum Mechanics and Thermodynamics*, pages 1–9, 2011.

[14] H. K. D. H. Bhadeshia. Diffusional formation of ferrite in iron and its alloys. *Progress in Materials Science*, 29(4):321–386, January 1985.

[15] M. Hillert. Paraequilibrium. Technical report, Swedish Institute for Metals Research, Stockholm, Sweden, 1953.

[16] J. S. Kirkaldy. A Zener-Hillert model for growth of binary alloy cells. *Scripta Metallurgica*, 14(7):739–744, July 1980.

[17] G.R. Purdy, D H Weichert, and J. S. Kirkaldy. The Growth of Proeutectoid Ferrite in Ternary Iron-Carbon- Manganese Austenites. *Trans. AIME*, 230:1025–1034, 1964.

[18] D. E. Coates. Diffusional growth limitation and hardenability. *Metallurgical Transactions*, 4(10):2313–2325, October 1973.

[19] S.A. Al-Salman, G. W. Lorimer, and N. Ridley. Pearlite growth kinetics and partitioning in a Cr-Mn eutectoid steel. *Metallurgical Transactions A*, 10(11):1703–1709, 1979.

[20] J. Chance and N. Ridley. Chromium partitioning during isothermal transformation of a eutectoid steel. *Metallurgical and Materials Transactions A*, 12 A(7):1205–1213, July 1981.

[21] C. R. Hutchinson, R. E. Hackenberg, and G. J. Shiflet. The growth of partitioned pearlite in Fe–C–Mn steels. *Acta Materialia*, 52(12):3565–3585, July 2004.

[22] S. Lenka, S. Kundu, S. Chandra, and S. B. Singh. Effect of recalescence on microstructure and phase transformation in high carbon steel. *Materials Science and Technology*, 29:715–725, 2013.

[23] D. Luo, M. J. Peet, S. W. Ooi, P. Yan, Z. Yin, and H. K. D. H. Bhadeshia. Spheroidisation of hypereutectoid state of nanostructured bainitic steel. *Materials Science and Technology*, ??:DOI 10.1179/1743284714Y.0000000545, 2014.

[24] R. S. Qin, A. Rahnama, W. J. Lu, and B. Eliott-Bowman X. F. Zhang and. Electropulsed steels. *Materials Science and Technology*, 30:DOI 10.1179/1743284714Y.0000000533, 2014.

[25] M. M. Aranda, B. Kim, R. Rementeria, C. Capdevila, and C. Garcia de Andrés. Effect of prior austenite grain size on pearlite transformation in a hypoeuctectoid Fe-C-Mn steel. *Metallurgical & Materials Transactions A*, 45:1778–1786, 2014.

[26] R. T. van Tol, Zhao, and J. Sietsma. Kinetics of austenite decomposition in manganese-based steel. *Acta Materialia*, 64:33–40, 2014.

[27] J. Li and L. Wei. Effects of high magnetic field on isothermal pearlite transformation and microstructure in a hypereutectoid steel. *Journal of Magnetism and Magnetic Materials*, 362:159–164, 2014.

[28] H. C. Sorby. On the Application of Very High Powers to the Study of the Microscopical Structure of Steel. *J. Iron Steel Inst.*, 1(1):140–147, 1886.

[29] C. Benedicks. The Nature of Troostite. *J. Iron Steel Inst.*, 2:352–370, 1905.

[30] G. V. Smith and R. F. Mehl. Lattice Relationships In Decomposition Of Austenite To Pearlite, Bainite, And Martensite . *Trans. AIME*, 150:211–226, 1942.

[31] F. C. Hull, R. A. Colton, and R. F. Mehl. Rate of Nucleation and Rate of Growth of Pearlite. *Trans. AIME*, 150:185, 1942.

[32] S. Modin. The isothermal transformation of austenite in carbon steels containing 0.50 percent C and 0.18 percent C. *Jernkontorets Ann.*, 142:37, 1958.

[33] H. K. D. H. Bhadeshia and R. Honeycombe. *Steels: microstructure and properties?* Elsevier Science & Tech, 3rd edition, 2006.

[34] K. M. Wu and H. K. D. H. Bhadeshia. Extremely fine pearlite by continuous cooling transformation. *Scripta Materialia*, 67(1):53–56, July 2012.

[35] P. R. Howell. The Pearlite Reaction in Steels Mechanisms and Crystallography. *Materials Characterization*, 40(4-5):227–260, April 1998.

[36] G. F. Bolling and R. H. Richman. Forced Velocity Pearlite. *Metallurgical and Materials Transactions B*, 1(8):2095–2104, 1970.

[37] D. D. Pearson and J. D. Verhoeven. Forced Velocity Pearlite in High Purity Fe-C Alloys: Part 1. Experimental. *Metallurgical and Materials Transactions A*, 15:219–224, 1984.

[38] M. Hillert. An analysis of the effect of alloying elements on the pearlite reaction. *Solid to Solid Phase Transformations*, pages 789–805, 1981.

[39] K. Kuo. Carbides in chromium, molybdenum and tungsten steels. *J. Iron Steel Inst.*, 173:363–375, 1953.

[40] J. W. Cahn and W. C. Hagel. Theory of Pearlite Reaction. In V F Zackay and H I Aaronson, editors, *Decomposition of Austenite by Diffusional Processes*, pages 131–192, New York, 1962. Intersciences.

[41] J-O. Andersson, T. Helander, L. Höglund, P. Shi, and B. Sundman. Thermo-Calc & DICTRA, computational tools for materials science. *Calphad-Computer Coupling Of Phase Diagrams And Thermochemistry*, 26(2):273–312, June 2002.

[42] D. S. Zhou and G. J. Shiflet. Ferrite: Cementite crystallography in pearlite. *Metallurgical and Materials Transactions A*, 23(4):1259–1269, April 1992.

[43] S. Z. Bokshteyn. Diffusion and the structure of metals. *Metal Science And Heat Treatment*, 3(11-12):473–480, 1961.

[44] J. Ågren. A revised expression for the diffusivity of carbon in binary FeC austenite. *Scripta Metallurgica*, 20(11):1507–1510, November 1986.

[45] R. Trivedi and G. M. Pound. Effect of concentration dependent diffusion coefficient on the migration of interphase boundaries. *Journal Of Applied Physics*, 38:3569–3576, 1967.

[46] L. Kaufman, P. Turchi, W. M. Huang, and Z. K. Liu. Thermodynamics of the Cr-Ta-W system by combining the ab initio and CALPHAD methods. *Calphad-Computer Coupling Of Phase Diagrams And Thermochemistry*, 25(3):419–433, 2001.

[47] H. K. D. H. Bhadeshia. Diffusion of carbon in austenite. *Metal Science*, 15(10):477–480, October 1981.

[48] R. H. Siller and R. B. McLellan. The Variation with Composition of the Diffusivity of Carbon in Austenite. *Trans. Met. Soc. AIME*, 245:697, 1969.

[49] R. P. Smith. Equilibrium of Iron-Carbon Alloys with Mixtures of CO-CO2 and CH4-H2. *Journal of the American Chemical Society*, 68(7):1163–1175, July 1946.

[50] R. B. McLellan and W. W. Dunn. A quasi-chemical treatment of interstitial solid solutions: It application to carbon austenite. *Journal of Physics and Chemistry of Solids*, 30(11):2631–2637, November 1969.

[51] J. S. Fisher, J. H. Holloman, and D. Turnbull. Institute of Metals Division - Kinetics of the Austenite-Martensite Transformation. *Trans. Met. Soc. AIME*, 175:202, 1948.

[52] R. S. BARNES. Diffusion of Copper along the Grain Boundaries of Nickel. *Nature*, 166(4233):1032–1033, December 1950.

[53] A. D. Le Claire. Grain boundary diffusion in metals. *Philosophical Magazine Series 7*, 42(328):468–474, 1951.

[54] J. Fridberg, L. E. Torndahl, and M. Hillert. Diffusion in Iron. *Jernkontorets Annaler*, 153(6):263–276, 1969.

[55] B. L. Bramfitt and A. R. Marder. A Transmission-Electron-Microscopy Study of the Substructure of High-Purity Pearlite. *Metallography*, 6(6):483–495, 1973.

[56] J. D. Verhoeven. Forced velocity pearlite in high purity Fe-C alloys: Part II. Theoretical. *Metallurgical and Materials Transactions A*, 1984.

[57] N. A. Razik, G. W. Lorimer, and N. Ridley. Chromium Partitioning During the Austenite-Pearlite Transformation. *Metallurgical Transactions A*, 7(2):209–214, 1976.

[58] D. Turnbull. Theory of cellular precipitation. *Acta Metallurgica*, 3(1):55–63, January 1955.

[59] W. Seith and F. G. Laird. Diffusion of Metals in Solid Lead . *Ztsch. Metallkunde*, 24:193, 1932.

[60] I. Steinbach and M. Apel. The influence of lattice strain on pearlite formation in Fe–C. *Acta Materialia*, 55(14):4817–4822, August 2007.

[61] D. Brown and N. Ridley. Kinetics of the pealite reaction in high-purity nickel eutectoid steels. *Journal of Iron and Steel Institute*, 207:1232–1240, 1969.

[62] D. E. Coates. Diffusion-controlled precipitate growth in ternary systems I. *Metallurgical Transactions*, 3(5):1203–1212, May 1972.

[63] D. E. Coates. Diffusion controlled precipitate growth in ternary systems: II. *Metallurgical Transactions*, 4(4):1077–1086, April 1973.

[64] J. S. Kirkaldy. Diffusion in multicomponent metallic systems: I. phenomenological theory for substitutional solid solution alloys. *Canadian Journal of Physics*, 36(7):899–906, July 1958.

[65] F. S. Ham. Shape-preserving solutions of the time-dependent diffusion equation. *Quart. Appl. Math.*, 17(2):137, 1959.

[66] M. L. Picklesimer, D. L. McElroy, T. M. Kegley, and J. H. Frye. Effect of Manganese on the Austenite-Pearlite Transformation. *Trans. Met. Soc. AIME*, 218:473–480, 1960.

[67] N. A. Razik, G. W. Lorimer, and N. Ridley. An Investigation of Manganese Partitioning During the Austenite-Pearlite Transformaion Using Analytical Electron Microscopy. *Acta Metallurgica*, 22:1249–1258, March 1974.

[68] R. F. Mehl and W. C. Hagel. The austenite: Pearlite reaction. *Progress in Metal Physics*, 6:74–134, January 1956.

[69] J. W. Cahn and W. G. Hagel. Divergent pearlite in a manganese eutectoid steel. *Acta Metallurgica*, 11(6):561–574, June 1963.

[70] J. E. Hillard and J. W. Cahn. An Evaluation of Procedures in Quantitative Metallography for Volume-Fraction Analysis. *Trans. Met. Soc. AIME*, 221:344, 1961.

[71] W. A. Johnson and R. F. Mehl. Reaction kinetics in processes of nucleation and growth. *Trans. AIME*, 135:416–458, 1939.

[72] S. E. Offerman, L. J. G. W. Van Wilderen, N. H. Van Dijk, J. Sietsma, M. T. Rekveldt, and S. Van der Zwaag. In-Situ Study of Pearlite Nucleation and Growth During Isothermal Austenite Decomposition in Nearly Eutectoid Steel. *Acta Materialia*, 51(13):3927–3938, 2003.

[73] S. E. Offerman, N. H. Van Dijk, J. Sietsma, S. Grigull, E. M. Lauridsen, L. Margulies, H. F. Poulsen, M. T. Rekveldt, and S. Van der Zwaag. Grain Nucleation and Growth During Phase Transformations. *Science*, 298(5595):1003–1005, 2002.

[74] J. H. Frye Jr, E. E. Stansbury, and D. L. McElroy. Absolute Rate Theory Applied to Rate of Growth of Pearlite. *Trans. AIME*, 197:219–224, 1953.

[75] J. J. Kramer, G. M. Pound, and R. F. Mehl. The free energy of formation and the interfacial enthalpy in pearlite. *Acta Metallurgica*, 6(12):763–771, December 1958.

[76] S. K. Das, A. Biswas, and R. N. Ghosh. Volume fraction dependent particle coarsening in plain carbon steel. *Acta Metallurgica et Materialia*, 41(3):777–781, March 1993.

[77] P. Deb and M. C. Chaturvedi. Coarsening behavior of cementite particles in a ferrite matrix in 10B30 steel. *Metallography*, 15(4):341–354, December 1982.

[78] M. Ruda, D. Farkas, and G. Garcia. Atomistic simulations in the Fe–C system. *Computational Materials Science*, 45(2):550–560, April 2009.

[79] N. Ridley and D. Burgess. Partitioning of Co during pearlite growth in a eutectoid steel. *Metal Science*, 18(1):7–12, January 1984.

[80] W.-S. Ko, J.-Y Oh, J.-H. Shim, J.-Y. Suh, W. Y. Yoon, and B.-J. Lee. Design of sustainable V-based hydrogen separation membranes based on grain boundary segregation. *International Journal of Hydrogen Energy*, 39(23):12031–12044, August 2014.

[81] K. H. Xue, P. Blaise, L. Fonseca, G. Molas, E. Vianello, B. Traoré, B. De Salvo, G. Ghibaudo, and Y. Nishi. Grain boundary composition and conduction in HfO2: An ab initio study. *Applied Physics Letters*, 102(20):201908, May 2013.